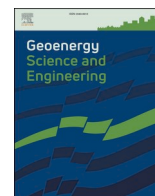


AMINAHO, E.N., HOSSAIN, M., FAISAL, N.H. and SANAAEE, R. 2024. Formation integrity evaluation for geosequestration of CO₂ in depleted petroleum reservoirs under cyclic stress conditions. *Geoenergy science and engineering* [online], 238, article number 212892. Available from: <https://doi.org/10.1016/j.geoen.2024.212892>

Formation integrity evaluation for geosequestration of CO₂ in depleted petroleum reservoirs under cyclic stress conditions.

AMINAHO, E.N., HOSSAIN, M., FAISAL, N.H. and SANAAEE, R.

2024



Formation integrity evaluation for geosequestration of CO₂ in depleted petroleum reservoirs under cyclic stress conditions

Efenwengbe Nicholas Aminaho^{a,*}, Mamdud Hossain^a, Nadimul Haque Faisal^a, Reza Sanaee^{a,b}

^a Robert Gordon University, School of Engineering, Aberdeen, United Kingdom

^b COWI, United Kingdom

ARTICLE INFO

Keywords:

Cyclic
Injection
Withdrawal
Geosequestration
Brittleness index
Dual-tubing string

ABSTRACT

The geological storage of carbon dioxide (CO₂), also referred to as CO₂ geosequestration, represents one of the most promising options for reducing greenhouse gases in the atmosphere. However, most of the time, CO₂ is captured with small amounts of other industrial gases such as sulphur dioxide (SO₂) and hydrogen sulphide (H₂S), which might be compressed together and stored in depleted petroleum reservoirs or aquifers. Moreover, during CO₂ geosequestration in reservoirs, pressure variations during injection could force some amount of CO₂ (with or without other acid gas impurities) into the caprock; thereby, altering the petrophysical, geochemical, and geomechanical properties of the caprock. Thus, the brittleness index of the reservoir and caprock might be impacted during CO₂ geosequestration due to the chemical reactions between the rock minerals and the formation fluid. Furthermore, to meet the world net-zero carbon target, the promotion of CO₂ utilization is paramount. This could be possible by developing an effective technology for cyclic CO₂ geosequestration (with or without gas impurities). Therefore, studies on the co-injection of CO₂ with other acid gases from industrial emissions, their withdrawal from the porous medium, and their impact on reservoir and caprock integrity are paramount. In this study, a dual-tubing string well completion technology was designed for cyclic injection and withdrawal of CO₂ (with or without another acid gas), and numerical simulations were performed using TOUGHREACT codes, to model the cyclic process and investigate the co-injection of SO₂ and H₂S (separately) with CO₂ in sandstone formations overlain by shale caprock. A novel technique of converting the volume fraction of minerals to their weight fraction was developed in this study, to evaluate the brittleness index of the sandstone reservoir and shale caprock during CO₂ geosequestration. The findings of the study indicate that the porosity and permeability increase for the CO₂ only and CO₂-H₂S injection cases, in the shale caprock; while for the CO₂-SO₂ injection case, porosity and permeability only decreased in the layers of the shale caprock contacted by SO₂ and due to anhydrite precipitation. In all the injection cases, the porosity and permeability of the sandstone reservoir decreased in a few layers directly below the perforation interval of the production zone. However, in other regions in the sandstone reservoir, the porosity and permeability increased for the CO₂ only and CO₂-H₂S injection cases. In contrast, for the CO₂-SO₂ co-injection case, porosity and permeability decreased in the layers of the sandstone rock contacted by SO₂. In all the CO₂ geosequestration cases, the brittleness of the shale and sandstone rocks investigated decreased slightly, except in the CO₂-SO₂ co-injection case where the brittleness of the sandstone rock decreased significantly. Based on the mineralogical composition of the formations in this study, co-injection of SO₂ gas with CO₂ gas, only decreased the brittleness index of the shale caprock slightly, but significantly decreased the brittleness of the sandstone reservoir.

1. Introduction

Carbon dioxide (CO₂) geosequestration represents one of the most promising options for reducing atmospheric emissions of CO₂ (Bachu,

2002). It has been proposed as one solution to global climate change caused by the heat-trapping of anthropogenic gases in the atmosphere (Wei et al., 2015; Klokov et al., 2017; Liu et al., 2020). What is fascinating about geosequestration is that CO₂ can be stored underground in

* Corresponding author.

E-mail addresses: aminahonicholas@gmail.com (E.N. Aminaho), m.hossain@rgu.ac.uk (M. Hossain), N.H.Faisal@rgu.ac.uk (N.H. Faisal), rese@cowi.com (R. Sanaee).

<https://doi.org/10.1016/j.geoen.2024.212892>

Received 19 October 2023; Received in revised form 28 March 2024; Accepted 3 May 2024

Available online 9 May 2024

2949-8910/© 2024 The Authors. Published by Elsevier B.V. This is an open access article under the CC BY-NC-ND license (<http://creativecommons.org/licenses/by-nc-nd/4.0/>).

caverns (salt caverns or engineered caverns) or porous media (aquifer and depleted oil or gas reservoirs). For long-term storage of gases, underground storage in aquifers or depleted oil (or gas) reservoirs is preferable due to the large storage capacity of gases in aquifers and depleted oil or gas reservoirs (Panfilov, 2016). Nonetheless, caprock integrity ascertained based on its petrophysical, geochemical, and geo-mechanical properties is vital to ensuring safe and sustainable storage of CO₂ (Pearce et al., 2016; Liu et al., 2020).

Meanwhile, CO₂ geosequestration could involve a non-cyclic or cyclic process. On the one hand, the non-cyclic process entails the injection of CO₂ over a period, then stopping the injection and allowing the injected CO₂ to be trapped in the reservoir. On the other hand, the cyclic process of geosequestration involves the injection of CO₂ for some period (in some cases, withdrawing some of the injected CO₂ and leaving behind some amount of CO₂ in the reservoir), and repeating the process over the geosequestration period. Cyclic injection and withdrawal of CO₂ in reservoirs might be an effective technology to promote CO₂ utilization, as this technology would enable seasonal injection and withdrawal of CO₂. Following this approach, CO₂ can be produced from the reservoir when needed for electrochemical hydrogen production (Kim et al., 2018; Koomson et al., 2023), to produce renewable methanol (Sánchez-Díaz, 2017; Sollai et al., 2023; Wang et al., 2023), in CO₂ plume geothermal (CPG) systems for heat and power production (Schifflechner et al., 2022), or other forms of energy. Thus, the utilization of CO₂ for energy creation will reduce the world's reliance on fossil fuels (Wang et al., 2023). The cyclic injection and withdrawal of CO₂ will promote its storage and utilization.

CO₂ storage is possible by its different trapping mechanisms including solubility trapping, residual trapping, mineral trapping, and structural/stratigraphic trapping mechanisms (Sun et al., 2016). The purity of the injected fluid influences brine-rock interactions during CO₂ geosequestration. To save the cost of carbon capture and storage, small amounts of some other acid gases (such as SO₂ and H₂S) may be co-injected with CO₂. When the gas mixture comes into contact with water, each gas in the mixture exhibits a different level of solubility in water due to differences in their polarity and net dipole moment (López-Rendón and Alejandre, 2008; Miri et al., 2014; Wang et al., 2020). Theoretically, water (H₂O), SO₂, and H₂S are polar molecules (electrons are not shared equally between the atoms and there is an electronegativity difference between the bonded atoms), while CO₂ is a linear non-polar molecule and the electrons are shared equally between the atoms (López-Rendón and Alejandre, 2008; Wang et al., 2020). Thus, CO₂ has no net dipole moment (as the two C–O bond dipoles are equal in magnitude and cancel out each other); while the dipole moments of H₂S, SO₂, and H₂O are 0.97 Debye, 1.63 Debye, and 1.83 Debye, respectively (López-Rendón and Alejandre, 2008; Shen et al., 2015; Wang et al., 2020). Also, substances whose polarities (or net dipole moment) are similar tend to be more soluble in each other, and a polar substance is more soluble in a polar solvent than in a non-polar solvent (López-Rendón and Alejandre, 2008; Wang et al., 2020). Thus, for the same initial amount of CO₂ at the same temperature and pressure conditions, the solubility of H₂S or SO₂ in water is higher than that of CO₂ (López-Rendón and Alejandre, 2008; Miri et al., 2014; Wang et al., 2020). Moreover, it is expected that the solubility of SO₂ in water should be higher than that of H₂S at the same temperature and pressure conditions, as the dipole moment of SO₂ is closer to that of water. Also, the solubility of gases in water is dependent on temperature; as temperature increases, the solubility of CO₂, H₂S, or SO₂ in water increases (López-Rendón and Alejandre, 2008; Miri et al., 2014).

It is worth noting that a gas can separate from a mixture with non-polar gases, due to their difference in property. This concept drives the industrial separation of SO₂/CO₂ in ionic liquid or aqueous phase (Wang et al., 2020). However, the level of solubility of CO₂ or impurities in a brine-rock system or the separation of impurities from CO₂ might be different when gas mixtures are injected in a rock composed of different minerals, thereby resulting in the trapping of the dissolved gases in the

aqueous phase for mineral precipitation. More or less fraction of each gas in the mixture might dissolve in the aqueous phase at different temperature and pressure conditions. So, the solubility trapping of CO₂ in a brine-rock system would depend on the initial mineralogical composition of the formation.

Residual trapping of CO₂ increases during cyclic CO₂ injection (Herring et al., 2016; Edlmann et al., 2019). During cyclic CO₂ injection, about 40–50% of CO₂ can be stored mainly through residual and solubility trappings in the porous medium (Abedini and Torabi, 2014). Water alternating gas (CO₂) and CO₂ cyclic injection strategies provide significantly higher effective CO₂ storage capacities compared to the continuous CO₂ injection strategy (Li et al., 2021). However, residually trapped CO₂ might reconnect with injected CO₂ mainly close to the large pore clusters in subsequent injection cycles, as observed during cyclic hydrogen (H₂) injections (Lysy et al., 2023). Moreover, increased residual trapping of CO₂ during cyclic injection, could result in a reduction in effective permeability, thereby limiting flow and injectivity after several cycles of CO₂ injection (Edlmann et al., 2019).

The exposure of supercritical CO₂ in certain geologic materials may induce surface chemical reactions that are time-dependent (Herring et al., 2016). Thus, the surface chemical reactions can influence the pore structure of the rock, as dissolution-dominant reactions of rock minerals would result in increased porosity and permeability, while precipitation-dominant reactions would result in decreased porosity and permeability of the rock. Dissolution of primary minerals in carbonate rock increases the porosity and permeability of the rock (Wang et al., 2022; Fatima et al., 2021).

Bolourinejad and Herber (2014) conducted an experimental study on the storage of CO₂ and impurities in a depleted gas field in the northeast Netherlands. Experiments were conducted on Permian Rotliegend sandstone reservoir (no initial calcite content) and Zechstein caprock (anhydrite and carbonate component) core samples at 300 bar and 100 °C for 30 days. Anhydrite precipitation was observed in H₂S or SO₂ co-injection case with CO₂, as the geochemical reaction with the formation water provided additional sulphur; while anhydrite dissolved in the pure CO₂ injection case. Pyrite and halite precipitated for the CO₂–H₂S co-injection case. In the CO₂–SO₂ co-injection case, enhanced levels of dissolution of carbonate and feldspar minerals were observed due to the formation of sulphuric acid from the geochemical reaction. Furthermore, after CO₂ injection, the permeability of the reservoir samples increased by 10–30%; while the permeability of caprock samples increased by a factor of 3–10, which indicates a significantly higher increase in the permeability of the caprock samples compared to the sandstone reservoir rock samples. CO₂ co-injection with 5000 ppm H₂S (higher concentration of the gas impurity, different from the other cases with 100 ppm gas impurity) reduced the permeability of the reservoir and caprock samples significantly (due to significant halite precipitation and small amount of pyrite and anhydrite precipitation), while only minimal change in permeability (less than 3% increase in permeability of the sandstone reservoir sample, and an increase in permeability up to 30% in the caprock sample) was observed when the concentration of H₂S was reduced to 100 ppm as the dissolution of minerals resulted in corresponding precipitation of secondary minerals. It is worth noting that after 17 days of CO₂ co-injection with 100 ppm H₂S, the permeability of the reservoir and caprock samples decreased as the precipitation of halite dominated the dissolution of feldspar and carbonate minerals. However, over time, the mineral dissolution process dominated, resulting in an increase in permeability of the rock samples after 30 days. In the case of CO₂ co-injection with 100 ppm SO₂, the permeability of reservoir rock samples increased by a factor of 1.18–2.2, while the permeability of the caprock samples changed by a factor of 0.8–2.3 (permeability increased in caprock samples with a higher ratio of initial carbonate mineral concentration to anhydrite content, due to the carbonate dissolution). The increase in the permeability of the sandstone reservoir could be attributed to the lack of calcite (mineral) in the initial composition of the rock. Thus, the release of Ca²⁺ from dolomite

dissolution was not enough to precipitate a significant amount of anhydrite (which could have decreased the permeability of the reservoir rock in the CO₂-SO₂ case). So, the initial mineralogical composition of the rock, duration of the geochemical reactions, and concentration of impurities in a CO₂ gas stream in reservoir and caprock samples impact the amount of change in permeability of reservoir and caprock.

A similar experimental study was conducted by [Aminu et al. \(2018\)](#) to evaluate the effect of impurities on sandstone reservoir permeability. The impurities considered are NO₂, H₂S, and SO₂. The experiment was conducted at 70 °C and 140 bar for 9 months. They found that the effect of H₂S on the rock permeability is relatively small. CO₂ increased the reservoir rock permeability by 5.83%, while CO₂-H₂S increased it by 6.25%. CO₂ co-injection with SO₂ slightly decreased permeability by 6.25%; while CO₂ co-injection with NO₂ significantly decreased permeability by 41.67%. The changes in the rock permeability are significantly influenced by the dissolution and precipitation of existing rock minerals, as well as the precipitation of some secondary minerals. So, the CO₂-brine-rock interactions depend on the purity of the CO₂ gas as well as the initial mineralogical composition of the rocks. The changes in permeability and porosity result from the dissolution of these gases in water, thus reducing pH which enhances chemical reactions in the rock and results in the dissolution of minerals (such as ankerite, siderite, dolomite, etc.), and precipitation of minerals (such as pyrite, dawsonite, kaolinite, anhydrite, etc.) in the rock ([Li et al., 2016](#); [Pearce et al., 2016, 2019](#)).

[Elwegaa et al. \(2019\)](#) conducted a study on cyclic cold carbon dioxide injection for improved oil recovery from shale oil reservoirs. They found that injection of cold CO₂ increased both porosities and permeabilities of the core samples by up to 3.5% and 8.8%, respectively. The porosity and proportion of macropores of coal (carbonate-rich rock) increase after treatment on cyclical injection of supercritical CO₂, as new pores were formed and some small pores possibly converted into macropores ([Su et al., 2021](#)). Moreover, the microporosity of sandstone increases during the cyclic wetting-drying process, similar to cyclic CO₂ injection, as the microstructure of the rock changes. The driving force of the changes in the microstructure of the sandstone is water-rock interaction including physical, mechanical, and chemical interactions ([Ke et al., 2023](#)). The chemical interaction that causes the dissolution and precipitation of some minerals in the rock can increase or decrease the porosity of the rock. For instance, in a study conducted by [Badrouchi et al. \(2022\)](#), after four CO₂ injection cycles, the effective porosity of the rock samples decreased, as the dissolved CO₂ could react with rock minerals and form precipitates that block some pores. These changes in the microstructure impact the petrophysical (porosity and permeability) and mechanical (elastic and strength parameters) properties of the rock. The strength and elastic (or deformation) parameters of the rock are dependent on its mineral compositions ([Li et al., 2023](#)). The change in the strength and elastic parameters (Young's modulus and Poisson's ratio) as the mineral compositions of the rock change during cyclic injection of CO₂ ([Su et al., 2020](#); [Xu et al., 2021](#)) could impact the brittleness of the reservoir and cap rocks.

[Elwegaa et al. \(2019\)](#) conducted a study on cyclic cold carbon dioxide injection for improved oil recovery from shale oil reservoirs. They observed an increase in the brittleness indices of the core samples. However, in the study, cold CO₂ was injected into the shale rock (reservoir), and brittleness index was calculated mainly by the ratio of the sum of the volume fractions of quartz and dolomite (which are not the only major brittle minerals in the rock samples); and the brittleness ratio was evaluated based on dynamic elastic modulus and Poisson's ratio, which do not accurately reflect the brittleness of rocks ([Meng et al., 2015](#); [Zhang et al., 2016](#)). Moreover, [Lyu et al. \(2018\)](#) developed a damage constitutive model for the effects of CO₂-brine-rock interactions on the brittleness of a low-clay shale (tested in a non-cyclic injection process). They found that the CO₂-brine-shale interactions in the soaked shale sample decreased the brittleness values. Therefore, the development of a more robust mathematical model to evaluate the brittleness of

reservoir and cap rocks during the non-cyclic and cyclic CO₂ injection process is paramount.

Previous studies have considered the impact of CO₂ and impurities (H₂S, SO₂, or NO₂) on porosity, permeability, and mineralogical changes in different rock lithologies, as well as the impact of pure CO₂-brine interaction on geomechanical properties and brittleness of rocks. Furthermore, several studies on the cyclic approach of CO₂ geosequestration have been based on CO₂ injection as a drainage-imbibition process in which case CO₂ is injected followed by water, from the same end of the rock sample and similar to water alternating gas approach of enhanced oil recovery; or periodic injection of CO₂ and producing from the other end of the reservoir (in a cartesian coordinate system) or observing the impact of the injected CO₂ in the reservoir. The cyclic injection-withdrawal of CO₂ during geosequestration is different in the present study.

In the present study, a novel approach of cyclic CO₂ geosequestration (with or without the addition of H₂S or SO₂ impurity) was developed to promote CO₂ utilization and storage by injecting CO₂ at the bottom of the well in a reservoir and producing CO₂ from the top part of the reservoir using the same well for both operations, to save cost and produce a purer form of CO₂. The proposed technology could be replicated on a laboratory scale by injecting CO₂ from one end of a water-saturated rock sample, followed by the injection of water from the other end of the rock sample [after the CO₂ injection period], making a cycle. This cycle can be repeated and therefore referred to as cyclic injection-withdrawal of CO₂ in the present study. This technology can be applied to several wells in the same reservoir, enabling the production of a purer form of CO₂ (with minimal chance of producing a large amount of brine together with the gas) as a larger amount of gas is few meters away (laterally) from the injection zone and at the top part of the reservoir; while multiphase mixture of CO₂-brine is found farther away from the injection well with a thin layer at the top of the reservoir having relatively low amount of CO₂ gas. Therefore, producing CO₂ gas from the same well used for injection, would save cost and enhance the production of a purer form of CO₂ for the development of renewable resources or energy (CO₂ utilization for hydrogen and methanol production, as well as for heat and power generation).

Also, to the best knowledge of the authors, no study has been conducted to investigate the impact of CO₂ impurities (H₂S or SO₂) on the brittleness of reservoir or cap rocks during cyclic CO₂ injection and withdrawal from the same wells and enabling CO₂ storage at the same time. Therefore, it is against this background that the authors have conceived the idea to design a dual-tubing string well completion approach for cyclic injection and withdrawal of CO₂ and evaluate the impact of CO₂ impurities on the brittleness of reservoir and cap rocks under cyclic stress conditions, during CO₂ geosequestration. This study investigates the impact of CO₂ impurities on the porosity, permeability, geochemical composition, and brittleness index of a sandstone reservoir and shale caprock during underground injection, withdrawal, and storage of CO₂. This study adopted a novel technique for converting the volume fraction of minerals to weight fraction for the evaluation of the brittleness index of rocks.

2. Theoretical framework

During CO₂ injection, stresses are induced in the rock as the cement that binds the rock grains are impacted. Thus, creating pathways for CO₂-brine-rock interaction in the [rock] cement and enhancing the dissolution of some of its minerals. Hence, resulting in deformation and a decrease in strength of the rock. The decrease in strength of the rock results in a change in the brittleness of the rock, as the rate of decrease in the tensile and compressive strengths of the rock, as well as changes in the rock minerals are different. Brittleness is the lack of ductility or plasticity of a material, while ductility is the property of a material that allows it to be drawn out by tension to a smaller section ([Hucka and Das, 1974](#); [Hou et al., 2018](#)). In other words, brittle materials can hardly be

drawn into shapes. Instead, they fracture or break when such an amount of stress is applied to them. Most rocks exhibit brittle behaviour. However, their degrees of brittleness vary by lithology and conditions subjected to during fluid-rock interactions.

Brittleness is a relative term as there are no accepted values of strength and elastic parameters ratios or brittle minerals ratio below which a material is considered ductile and above which it is considered as brittle (Hucka and Das, 1974). The brittleness of a material is compared by its brittleness index at one time or condition to another to ascertain whether the material has become more or less brittle. The factors that influence the brittleness of rocks include the type and composition of brittle minerals, the content and maturity of organic matter, and the formation temperature and confining pressure (Meng et al., 2015; Li, 2022). The brittleness index of rocks can be expressed based on rock strength parameters (Hucka and Das, 1974; Gong and Zhao, 2007; Meng et al., 2015; Li, 2022), elastic parameters (Rickman et al., 2008; Luan et al., 2014; Kang et al., 2020), and weight fraction of rock minerals (Jin et al., 2015; Guo et al., 2016; Kang et al., 2020; Li, 2022). Based on these parameters, the brittleness index of rocks is expressed as follows:

$$BI_1 = \frac{\sigma_c}{\sigma_t} \quad (1)$$

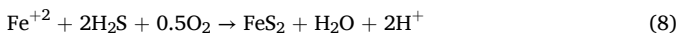
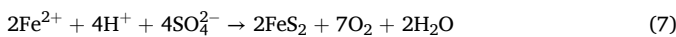
$$BI_2 = \frac{(\sigma_c - \sigma_t)}{(\sigma_c + \sigma_t)} \quad (2)$$

$$BI_3 = \frac{E}{\nu} \quad (3)$$

$$BI_4 = \frac{W_{quartz} + W_{feldspar} + W_{calcite} + W_{dolomite} + W_{pyrite} + W_{mica}}{W_T} \quad (4)$$

$$BI_5 = \frac{W_{quartz} + 0.49W_{feldspar} + 0.51W_{calcite} + 0.44W_{dolomite}}{W_T} \quad (5)$$

where σ_c represents uniaxial compressive strength and σ_t represents uniaxial tensile strength of the rock; E and ν represent Young's modulus and Poisson's ratio of the rock, respectively; W and W_T represent weight (or mass) of individual mineral and total weight (or mass) of minerals in the solid part of the rock, respectively; and specifically, BI_5 is mineralogical brittleness index developed by Kang et al. (2020) based on the bulk modulus of brittle minerals. Generally, brittle minerals include quartz, feldspar group of minerals, calcite, dolomite, pyrite, and mica. Fluid-rock interaction results in dissolution and precipitation of minerals, thereby altering the amount of brittle minerals in the rock. In the case of co-injection of CO₂ with SO₂, in the presence of water (H₂O) sulphates (or SO₄²⁻) are formed, resulting in the precipitation of anhydrite (CaSO₄) and some amount of pyrite (FeS₂); while co-injection of CO₂ with H₂S in the presence of oxygen and increased iron (Fe) concentration (possibly due to the dissolution of siderite and/or ankerite) could result in the precipitation of pyrite (Hedayati et al., 2018) as follows:



Therefore, the co-injection of gases (H₂S, SO₂, etc.) during CO₂ geosequestration may impact the brittleness of porous rocks as brittle and non-brittle minerals are precipitated during the co-injection of CO₂ with different impurities. Hence, it is vital to evaluate the impact of CO₂ impurities on the brittleness of rocks during geosequestration.

3. Methodology

The research design involves numerical simulations. Numerical

simulations were performed by modelling cyclic injection-withdrawal technology during CO₂ geosequestration. This strategy involves numerical simulations using sandstone formation as reservoir and shale formation as caprock, to model the process of cyclic injection-withdrawal of CO₂ in the reservoir. The results of the numerical simulations were analyzed for the brittleness index using the mathematical model developed by Aminaho and Hossain (2023). The mathematical model and the simulation approach are presented in this section.

3.1. Mathematical modelling

Change in the porosity of rocks is calculated based on mineral precipitation and dissolution, while the change in permeability is calculated from Carman-Kozeny relation, using the following equations (Xu et al., 2006, 2014):

$$\phi = 1 - \sum_{m=1}^{nm} fr_m - fr_u \quad (9)$$

$$k = k_0 \left(\frac{1 - \phi_0}{1 - \phi} \right)^2 \left(\frac{\phi}{\phi_0} \right)^3 \quad (10)$$

where, ϕ and k represent current porosity and permeability, ϕ_0 and k_0 represent initial porosity and permeability, parameters fr_m and fr_u represent volume fraction of mineral m in the rock (volume of mineral to volume of the medium including porosity) and volume fraction of non-reactive mineral, respectively. So, the output volume fraction of each mineral is the volume of the mineral divided by the volume of the medium including porosity (V_{frac}). Thus, the volume of each mineral divided by the total volume of the solid [part of the rock] is calculated as follows (Xu et al., 2014):

$$f_m = \frac{V_{frac}}{1 - \phi_{med}} \quad (11)$$

where ϕ_{med} represents [current] porosity of the medium, and f_m represents the volume of mineral per volume of [the solid part of] the rock.

The mass fraction of composite materials has been calculated to determine their mechanical properties (Ezema et al., 2015) using their densities and volume fractions. Therefore, it is possible to determine the mass fraction of minerals in a rock using a similar approach. The mass fraction of each material that forms a composite structure is the mass of that material to the total mass of materials that form the structure. Similarly, the mass fraction of each mineral that forms a rock is the mass of each mineral to the total mass of minerals that form the rock and can be expressed as follows:

$$\text{Mass fraction of a mineral, } x_i = \frac{\text{mass of the mineral,}}{\text{total mass of minerals in the rock,}} = \frac{m_i}{\sum_{i=1}^{nm} m_i} \quad (12)$$

$$m = V\rho \quad (13)$$

$$x_i = \frac{v_i \rho_i}{\sum_{i=1}^{nm} v_i \rho_i} \quad (14)$$

where V and ρ represent the volume and density of the solid, respectively; v_i represents the volume fraction of each mineral in the solid part of the rock (same as f_m). Density can be expressed as molecular weight divided by molar volume.

$$\rho = \frac{\bar{M}}{\bar{V}} \quad (15)$$

Thus, the mass fraction becomes:

$$x_i = \frac{\frac{v_i \bar{M}_i}{V_i}}{\sum_{i=1}^{nm} \frac{v_i \bar{M}_i}{V_i}} \quad (16)$$

where \bar{M} and \bar{V} represent molecular weight (g/mol) and molar volume (m^3/mol) of mineral. Hence, the mineralogical brittleness index by a simple sum of brittle minerals becomes:

$$BI_{min} = \frac{\sum_{j=1}^{nB} \frac{v_j \bar{M}_j}{V_j}}{\sum_{i=1}^{nm} \frac{v_i \bar{M}_i}{V_i}} \quad (17)$$

where j represents each brittle mineral in the rock, i represents any mineral in the rock, and nB represents the number of brittle minerals in the rock.

To simplify the derived brittleness index equation, the same molar volume can be assumed for all minerals, depending on the mineralogical composition of the rock. However, some clay minerals such as smectite-Ca, smectite-Na, illite, and kaolinite may have larger mineral surface areas (Fatah et al., 2022) and significantly different molar volumes. Assuming equal molar volume of minerals, the brittleness index in terms of the simple sum of brittle minerals in a rock can be expressed as:

$$BI_6 = \frac{\sum_{j=1}^{nB} v_j \bar{M}_j}{\sum_{i=1}^{nm} v_i \bar{M}_i} \quad (18)$$

Brittle minerals considered in this study are quartz, feldspar (as albite, k-feldspar, oligoclase, orthoclase, and anorthite), calcite, dolomite, pyrite, and mica (as muscovite). Their relative level of brittleness among themselves (brittle minerals) is not considered in the simple sum of brittle minerals approach given above. Thus, to consider their relative level of brittleness, the bulk modulus (Table 1) of the brittle minerals was incorporated into the equation using weighting coefficients (Table 2) following the mineralogical brittleness index developed by Kang et al. (2020).

The mineralogical brittleness index, considering the bulk modulus of minerals, developed by Kang et al. (2020) is given as:

$$BI_{BMod} = \frac{W_Q + 0.49W_F + 0.51W_C + 0.44W_D}{W_T} \quad (19)$$

where W_Q , W_F , W_C , and W_D represent the weights of quartz, feldspar, calcite, and dolomite, respectively; W_T represents the total mineral weight. The brittleness index in this case considers only quartz (Q), feldspar (F), calcite (C), and dolomite (D) as brittle minerals, assuming the level of brittleness of pyrite and mica is negligible compared to other brittle minerals. Thus, in the present study, the brittleness index becomes:

$$BI_{bm} = \frac{\frac{v_Q \bar{M}_Q}{V_Q} + \frac{0.49 v_F \bar{M}_F}{V_F} + \frac{0.51 v_C \bar{M}_C}{V_C} + \frac{0.44 v_D \bar{M}_D}{V_D}}{\sum_{i=1}^{nm} \frac{v_i \bar{M}_i}{V_i}} \quad (20)$$

So, assuming the same molar volume of minerals in this present study, the brittleness index can be expressed as:

Table 1
Bulk modulus of different brittle minerals (Fjaer et al., 2008).

Brittle mineral	Quartz	Feldspar	Calcite	Dolomite
Bulk modulus (GPa)	37.5	76	74	76–95

Table 2
Weighting coefficients of different brittle minerals (Kang et al., 2020).

Brittle mineral	Quartz	Feldspar	Calcite	Dolomite
Weighting coefficient	1	0.49	0.51	0.39-0.49/0.44

$$BI_7 = \frac{v_Q \bar{M}_Q + 0.49 v_F \bar{M}_F + 0.51 v_C \bar{M}_C + 0.44 v_D \bar{M}_D}{\sum_{i=1}^{nm} v_i \bar{M}_i} \quad (21)$$

The models developed in this study (accounting for the molar volume of each mineral and assuming the same molar volume for all minerals) are used to evaluate the mineralogical brittleness index of the sandstone reservoir and shale caprock before and after CO_2 geosequestration.

To test the statistical significance of differences in tests or observations at different stages or conditions, the concept of reliable change index (RCI) with 95% confidence (Blampied, 2016) can be adopted as follows:

$$RCI = 1.96(\sigma) \sqrt{2} \sqrt{(1-r)} \quad (22)$$

where, r and σ are Pearson correlation coefficient (or reliability index) and standard deviation of the variable dataset, respectively.

3.2. Numerical approach

This study employed the TOUGHREACT code for non-isothermal multiphase reactive geochemical transport (Xu et al., 2006), which was developed by incorporating reactive chemistry into TOUGH2 code for multiphase fluid and heat flow (Pruess, 2004). A detailed description of the TOUGHREACT code can be found in a study conducted by Zhang et al. (2011) and the program reference manual (Xu et al., 2014).

3.2.1. Model setup

A simple two-dimensional (2-D) radial well model was used in this study. The 2-D model is a vertically heterogeneous formation of 40 m thickness with a cylindrical geometrical configuration (Fig. 1). In the vertical direction, the model domain is discretized into 20 regular increments with a 2 m constant spacing (Δz). The top and bottom model boundaries are close to flow. The top model layers represent a shale caprock, while the remaining model layers at the bottom represent reservoir rock(s). The model layers are shown in Table 3.

In the horizontal direction, a 100 km radial distance was modelled with a radial grid spacing increasing logarithmically from the injection well. A total of 56 radial grid elements were generated. A large volume of 10^{30} m^3 is assigned to the outer grid element to represent an infinite lateral boundary (a constant hydrostatic pressure boundary). The interface between the reservoir and caprock in this study is 12 m from the top of the caprock considered in this model. The depleted petroleum reservoir considered in this study was assumed to be under a strong aquifer, such that a very large fraction of the hydrocarbon in the reservoir has been produced and the reservoir pore spaces were replaced by water. Therefore, the reservoir simulation is similar to CO_2 geosequestration in aquifers, which TOUGHREACT can handle effectively. Thus, the effect of hydrocarbon reactions with the injected gases and formation water were not considered in this study.

CO_2 only (also referred to as CO_2 alone, in this study) or impure CO_2 (containing H_2S or SO_2) injection was applied at the bottom of the well, and produced (or withdrawn) at the upper part of the well in the same reservoir (close to the caprock zone), to produce relatively pure CO_2 gas (and limit the production of aqueous-phase fluid). The thickness of the injection portion is 8 m, while the thickness of the production portion is 6 m as shown in Fig. 1.

The initial reservoir and caprock temperature and pressure are 40°C and 10 MPa (100 bar), respectively. The CO_2 injection-withdrawal profile is shown in Fig. 2. The injection-withdrawal process was

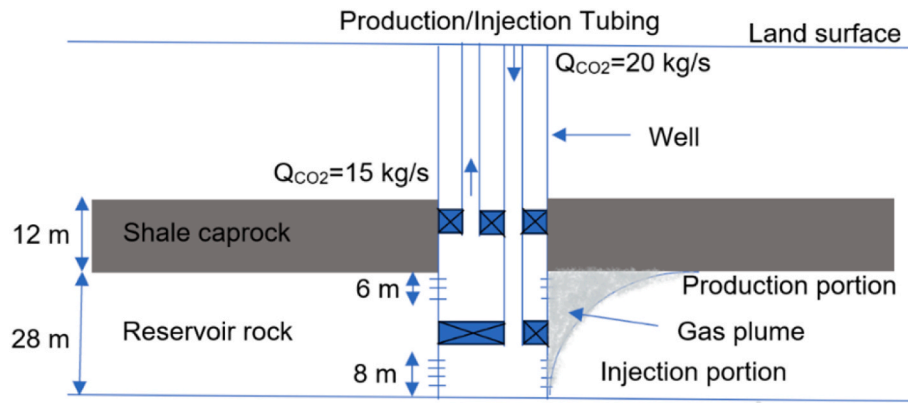
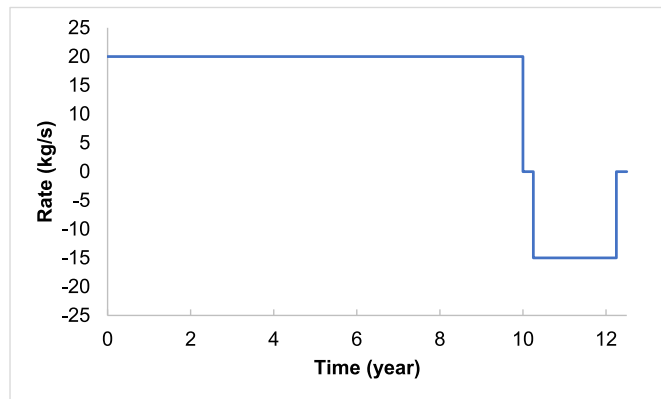
Fig. 1. Cyclic injection-withdrawal of CO₂.

Table 3
Mesh generation of the model.

Rock formation	Vertical mesh number	Mesh thickness (m)
Shale caprock	6	2.0
Sandstone reservoir	14	2.0

Fig. 2. CO₂ injection-withdrawal profile.

completed over seven (7) cycles. For each cycle, CO₂ gas (with or without H₂S/SO₂ gas) is injected (at the 8 m injection portion/zone) into the reservoir for a period of 10 years, using a CO₂ injection rate of 20 kg/s (with or without a gas impurity) and with a 0.025-mol fraction of H₂S or SO₂ (for the co-injection cases). The mole fraction of 0.025 for H₂S and SO₂ was selected as it is within the range of CO₂ co-capture from Pet Coke (SNC-Lavalin Inc, 2004). CO₂ injection is stopped for 3 months (0.25 year), then CO₂ is withdrawn from the reservoir at the rate of 15 kg/s (at the 6 m production portion/zone) over a period of 2 years and withdrawal is stopped for 3 months before the next cycle commences. So, each cycle lasted for 12.5 years. The longer period of production compared to the shut-in time is based on field applications of cyclic gas injection in reservoirs (Reeves, 2001). The hydrogeological parameters used in this study are shown in Table 4.

The initial mineralogical composition of the sandstone reservoir was obtained and modified from Zhang et al. (2011), while the initial mineralogical composition of the shale caprock was obtained and modified from Ma et al. (2019). The molar volumes of the minerals were obtained from Robie et al. (1967) and Wang et al. (2021), except the molar volumes of dawsonite, smectite-Ca and ankerite that were assumed. The molar volume of dawsonite was obtained from Marini (2007); the molar volume of smectite-Ca was estimated within the range of density of Smectites (2.6 g/cm³) (Deer et al., 1966; Totten et al.,

Table 4
Hydrogeological parameters used in the simulation at formation temperature and pressure of 40 °C and 100 bar, respectively.

Parameters	Formation	
	Sandstone	Shale caprock
Porosity	0.34	0.07
Horizontal permeability (m ²)	2.264 × 10 ⁻¹³	2.264 × 10 ⁻¹⁶
Vertical permeability (m ²)	2.264 × 10 ⁻¹⁴	2.264 × 10 ⁻¹⁷
Pore compressibility (Pa ⁻¹)	2.10 × 10 ⁻⁹	2.10 × 10 ⁻⁹
Rock grain density (kg/m ³)	2600	2600
Formation heat conductivity (W/m °C)	2.51	2.51
Rock grain specific heat (J/kg °C)	920.0	920.0
Temperature (°C)	40.0	40.0
Salinity (mass fraction)	0.06	0.06
Pressure (bar)	100	100
Initial gas saturation	0.00	0.00
CO ₂ injection rate (kg/s)	20.0	–
CO ₂ withdrawal rate (kg/s)	15.0	–
Relative permeability	$S^* = (S_i - S_{ir}) / (1 - S_{ir})$ $S_{ir} = 0.30$ $m = 0.457$ $\tilde{S} = (S_i - S_{ir}) / (1 - S_{ir} - S_{gr})$ $S_{gr} = 0.05$	
Liquid: Van Genuchten function $k_{rl} = \sqrt{S^* \{1 - (1 - [S^*]^{1/m})^m\}^2}$		
S_{ir} : residual water saturation m: exponent		
Gas: Corey $k_{rg} = (1 - \tilde{S})^2 (1 - \tilde{S}^2)$		
S_{gr} : residual gas saturation		
Capillary pressure	$S^* = (S_i - S_{ir}) / (1 - S_{ir})$ $S_{ir} = 0.03$ $m = 0.457$	
Van Genuchten function		
$P_{cap} = -P_0 ([S^*]^{-1/m} - 1)^{1-m}$		
S_{ir} : residual water saturation m: exponent		
P_0 : strength coefficient	19.61 kPa	19.61 kPa

2002), while the molar volume of ankerite was estimated using a density of 2.97 g/cm³ (Shafiq et al., 2022). The mineralogical compositions of the rocks are shown in Table 5.

Before the simulation of reactive transport, a batch geochemical modelling of water-rock interaction was performed to obtain an aqueous-phase chemical composition similar to the composition of a typical formation brine. So, synthetic brine formulated by AL-Ameri et al. (2016) with very little amount of other necessary ions based on the mineral compositions considered in the simulations was used. The synthetic brine was equilibrated separately for the different formations and injection conditions considered, in the presence of the primary minerals listed in Table 5. The batch geochemical modelling was conducted for 100 years to obtain a quasi-stable (or nearly steady-state) aqueous solution composition as shown in Table 6.

Dissolution and precipitation of minerals are considered under ki-

Table 5
Initial volume fractions of the minerals and their molecular weight and molar volume.

Mineral name	Chemical formula	Molecular weight (g/mol)	Molar volume (cm ³ /mol)	Sandstone formation (volume percent of solid)	Shale Caprock (volume percent of solid)
Illite	K _{0.6} Mg _{0.25} Al _{1.8} (Al _{0.5} Si _{3.5} O ₁₀)(OH) ₂	383.899	138.900	2.80	65.30
Kaolinite	Al ₂ Si ₂ O ₅ (OH) ₄	258.159	99.520	0.90	1.11
Smectite-Ca	Ca _{0.145} Mg _{0.26} Al _{1.77} Si _{3.97} O ₁₀ (OH) ₂	365.394	140.536	0	6.96
Chlorite	Mg _{2.5} Fe _{2.5} Al ₂ Si ₃ O ₁₀ (OH) ₈	634.648	210.260	2.70	6.40
Quartz	SiO ₂	60.084	22.688	25.80	8.00
K-feldspar	KAlSi ₃ O ₈	278.33	108.900	23.30	2.80
Albite	NaAlSi ₃ O ₈	262.222	100.070	41.50	3.20
Calcite	CaCO ₃	100.087	36.934	3.00	0.80
Pyrite	FeS ₂	119.98	23.940	0	1.43
Dolomite	CaMg(CO ₃) ₂	184.401	64.341	0	0
Anhydrite	CaSO ₄	136.142	45.940	0	4.00
Siderite	FeCO ₃	115.856	146.800	0	0
Alunite	KAl ₃ (OH) ₆ (SO ₄) ₂	414.214	69.522	0	0
Ankerite	CaMg _{0.3} Fe _{0.7} (CO ₃) ₂	206.48	58.520	0	0
Dawsonite	NaAlCO ₃ (OH) ₂	143.995	28.018	0	0
Magnesite	MgCO ₃	84.314	29.378	0	0
Smectite-Na	Na _{0.290} Mg _{0.26} Al _{1.77} Si _{3.97} O ₁₀ (OH) ₂	366.25	132.510	0	0
Hematite	Fe ₂ O ₃	159.692	30.274	0	0
Anorthite	CaAl ₂ Si ₂ O ₈	278.206	100.790	0	0
Muscovite	KAl ₂ (AlSi ₃ O ₁₀)(F,OH) ₂	398.306	140.710	0	0
Oligoclase	CaNa ₄ Al ₆ Si ₁₄ O ₄₀	1327.094	502.480	0	0

Table 6
Initial chemical composition of the formation water at formation conditions of 40 °C and 100 bar.

Component	Concentration (mol/kg H ₂ O)	
	Sandstone formation	Shale caprock
Ca ²⁺	4.7137E-01	4.8163E-01
Mg ²⁺	1.0038E-01	9.7547E-02
Na ⁺	2.5868E+00	2.6006E+00
K ⁺	2.8166E-03	3.3113E-03
Fe ²⁺	4.9784E-04	2.7904E-08
SiO ₂ (aq)	2.9555E-03	1.3991E-03
HCO ₃ ⁻	2.1733E-03	1.2688E-04
SO ₄ ²⁻	3.6425E-03	1.7486E-02
AlO ₂ ⁻	1.3611E-11	6.1835E-11
Cl ⁻	3.7245E+00	3.7264E+00
pH	6.1989	7.3919

netic conditions based on the rate law (Lasaga et al., 1994) expressed as:

$$r_n = \pm k_n A_n \left[1 - \left(\frac{Q_n}{K_n} \right)^\theta \right] \quad (23)$$

where k_n is the rate constant (in moles per unit mineral surface area and unit time) which is temperature-dependent, A_n denotes the specific reactive surface area per kilogram H₂O, Q_n is the reaction quotient, K_n is the equilibrium constant for the mineral-water written for the destruction of 1 mol of mineral n , and η represents kinetic mineral index. The parameters θ and η which are determined by experiments, are more often assumed to equal to one. Positive values of r_n indicate dissolution, while negative values indicate precipitation.

A general form of species-dependent rate constants implemented in TOUGHREACT is expressed as:

$$k = k_{25}^{nu} \exp \left[\frac{-E_a^{nu}}{R} \left(\frac{1}{T} - \frac{1}{298.15} \right) \right] + \sum_i k_{25}^i \exp \left[\frac{-E_a^i}{R} \left(\frac{1}{T} - \frac{1}{298.15} \right) \right] \prod_j a_{ij}^{\eta_{ij}} \quad (24)$$

where superscripts or subscripts i represents the additional mechanism index, and j represents the species index involved in one mechanism that could be primary or secondary species.

In this study, calcite and anhydrite are assumed to react with

aqueous species at local equilibrium. This is because the reaction rates of calcite and anhydrite are typically quite rapid (Zheng et al., 2009). The kinetic parameters were taken from Xu et al. (2006) and Zhang et al. (2011) and are shown in Table 7.

A temperature of 40 °C was used in the reservoir which may represent shallow formation temperature at a depth of about 800 m, given a land surface temperature of 16 °C and a geothermal gradient of 30 °C/km. The temperature in the reservoir and cap rocks are assumed to be initially the same as the rock thickness considered in the simulation is only 40 m. Also, the numerical simulations were conducted under isothermal condition.

3.2.2. Simulations

Three groups of numerical simulations were performed (as shown in Table 8) to investigate the effect of CO₂ injection or CO₂ co-injection with other gases (H₂S or SO₂) on the petrophysical (porosity and permeability) and geochemical (aqueous composition and mineral dissolution/precipitation) changes of the rocks, and evaluate the brittleness of the rocks during the cyclic technique of CO₂ geosequestration.

3.3. Model Validation

The numerical simulations performed and the mathematical model adopted for the evaluation of brittleness index of rocks in this study were validated using experimental data published by Mavhengere et al. (2022) on the influences of SO₂ contamination in long-term supercritical CO₂ treatment on the physical and structural characteristics of sandstone rock. Mavhengere et al. (2022) conducted two types of storage experiments on sandstone core samples (Cenomanian Sandstone, ZG and Siltstone lateral seal Aptian Sandstone, ZC) from Zululand Basin in South Africa, using pure CO₂ gas (purity of 99.9% by weight); and another case using a mixture of 99% (weight) CO₂ and 1% (weight) SO₂ gas. Non-stirred Teflon lined N4766 Parr reactors were used to simulate geosequestration conditions of 17.5 MPa and 346 K for the ZC core samples, and 10 MPa and 316K for the ZG core samples for 2 months. X-ray diffraction (XRD) analyses were conducted on the samples before and after treatment with CO₂ or CO₂-SO₂ mixture to investigate any mineral phase alterations. The ZC core sample exhibited mineral phase alteration after treatment (fluid-rock interaction) similar to the sandstone rock in the present study. Therefore, to validate the mathematical models adopted in the present study, to evaluate the impact of contaminant (SO₂) in CO₂ on the brittleness index of sandstone, the

Table 7

List of parameters for calculating the kinetic rate of minerals.

Mineral name	Initial reactive surface area (cm ² /g)	Neutral mechanism		Acid mechanism			Base mechanism		
		K ₂₅ (mol/m ² s)	E _a (kJ/mol)	K ₂₅ (mol/m ² s)	E _a (kJ/mol)	n (H ⁺)	K ₂₅ (mol/m ² s)	E _a (kJ/mol)	n (H ⁺)
Calcite	Assumed in equilibrium								
Anhydrite	Assumed in equilibrium								
Quartz	9.8	1.0233E-14	87.7						
Kaolinite	151.63	6.9183E-14	22.2	4.8978E-12	65.90	0.777	8.9125E-18	17.90	-0.472
Illite	151.63	1.6596E-13	35.00	1.0471E-11	23.6	0.34	3.02E-17	58.9	-0.40
Pyrite	12.87	2.8184E-05	56.90 n _{O2(aq)} = 0.5	3.02E-08	56.9	n _{H+} = -0.5 n _{Fe3+} = 0.5			
K-feldspar	9.8	3.8905E-13	38.0	8.7096E-11	51.7	0.5	6.3096E-22	94.1	-0.823
Dolomite	9.8	2.9512E-08	52.20	6.4565E-04	36.1	0.5			
Siderite	9.8	1.2598E-09	62.76	6.4565E-04	36.1	0.5			
Ankerite	9.8	1.2598E-09	62.76	6.4565E-04	36.1	0.5			
Albite	9.8	2.7542E-13	69.80	6.9183E-11	65.0	0.457	2.5119E-16	71.0	-0.572
Muscovite	9.8	3.160E-13	58.6						
Hematite	12.87	2.5119E-15	66.2	4.0738E-10	66.2	1.0			
Chlorite	9.8	3.020E-13	88.0	7.7624E-12	88.0	0.5			
Oligoclase	9.8	1.4454E-13	69.8	2.1380E-11	65.0	0.457			
Magnesite	9.8	4.5709E-10	23.5	4.1687E-07	14.4	1.0			
Dawsonite	9.8	1.2598E-09	62.76	6.4565E-04	36.1	0.5			
Smectite-Na	151.63	1.6596E-13	35.0	1.0471E-11	23.6	0.34	3.0200E-17	58.9	-0.40
Smectite-Ca	151.63	1.6596E-13	35.0	1.0471E-11	23.6	0.34	3.0200E-17	58.9	-0.40
Alunite	9.8	1.0000E-12	57.78				1.0000E-12	7.5	-1.00
Anorthite	9.8	1.5000E-14	18.4						

Table 8

Three groups of simulations in this study.

Simulation groups	Injection scenarios	Formation	Formation salinity
1	CO ₂ only	Sandstone and shale	0.06
2	CO ₂ and H ₂ S	Sandstone and shale	0.06
3	CO ₂ and SO ₂	Sandstone and shale	0.06

mineral phases (weight fraction) of the ZC core samples (shown in Table 9) were incorporated into existing models that are based on simple weight fraction of brittle minerals (Jin et al., 2015; Guo et al., 2016; Li, 2022) and weight fraction considering the relative brittleness of brittle minerals (Kang et al., 2020). In this case, the brittle minerals are quartz, plagioclase (feldspar), calcite, pyrite, and orthoclase (feldspar).

4. Results and discussion

4.1. Impact of impurities on porosity, permeability, and geochemical composition of reservoir and cap rocks during CO₂ injection, withdrawal, and storage

The supercritical CO₂ fluid (referred to as 'gas' in this study for simplicity) is injected or co-injected with H₂S (or SO₂) near the bottom

of the sandstone reservoir and withdrawn near the top of the reservoir, in a cyclic process (in a total of seven cycles). The injected fluid migrates rapidly upward by buoyant forces. After every cycle of injection, a small fraction of CO₂ gas is trapped in the reservoir as residual gas; while the mobile gas continues to migrate into the shale caprock by the action of buoyant forces. At the same time, some amount of the gas continues to dissolve into brine (formation water). Hence, the residual gas slowly disappears at the bottom of the reservoir. After some time, most of the free CO₂ gas accumulates in the shale caprock layers, a few metres from the reservoir-caprock interface, and spreads laterally. The SO₂ gas front is far behind that of CO₂ gas compared to the front of H₂S gas with respect to CO₂ gas as shown in Fig. 3. This is because the solubility of SO₂ gas in formation water is higher than that of H₂S and CO₂. This difference in their solubility level can be attributed to their difference in polarity and net dipole moment, as the net dipole moment of SO₂ is closer to that of water molecule, compared to the closeness of the net dipole moment of H₂S to water molecule (López-Rendón and Alejandre, 2008; Miri et al., 2014; Wang et al., 2020). However, some amount of H₂S gas and SO₂ gas remain in the reservoir even after the seventh cycle, as they continue to be replenished due to the cyclic injection process (Fig. 4).

Fig. 4 shows that H₂S gas hardly penetrated up to 4 m vertical thickness of the shale caprock, while SO₂ gas only penetrated up to 2 m vertical thickness of the caprock after seven (7) cyclic injection-withdrawal of CO₂ stream. Only CO₂ gas penetrated over 8 m vertical thickness of the shale caprock during the period of geosequestration.

There is no notable difference in the distribution of total dissolved

Table 9ZC and ZG core samples XRD results before and after ScCO₂-water and ScCO₂-SO₂-water treatment (Mavhengere et al., 2022).

Sample	Quartz (wt. %)	Plagioclase (wt. %)	Smectite (wt. %)	Calcite (wt. %)	Pyrite (wt. %)	Stilbite (wt. %)	Diopside (wt. %)	Gypsum (wt. %)	Orthoclase (wt. %)
ZC untreated	44.1	44.7	1.0	3.5	0.4	3.6	2.7	0.0	0.0
ZC CO ₂ treated	47.5	42.5	2.5	1.7	0.4	2.7	2.8	0.0	0.0
ZC CO ₂ -SO ₂ treated	49.1	28.6	11.8	0.0	0.8	4.9	2.3	2.5	0.0
ZG untreated	21.5	46.0	22.2	0.0	0.0	2.0	0.0	0.0	8.3
ZG CO ₂ treated	22.3	50.5	16.3	2.9	0.0	4.8	0.0	0.0	3.2
ZG CO ₂ -SO ₂ treated	26.1	53.4	12.1	2.3	0.0	0.0	0.0	0.0	6.2

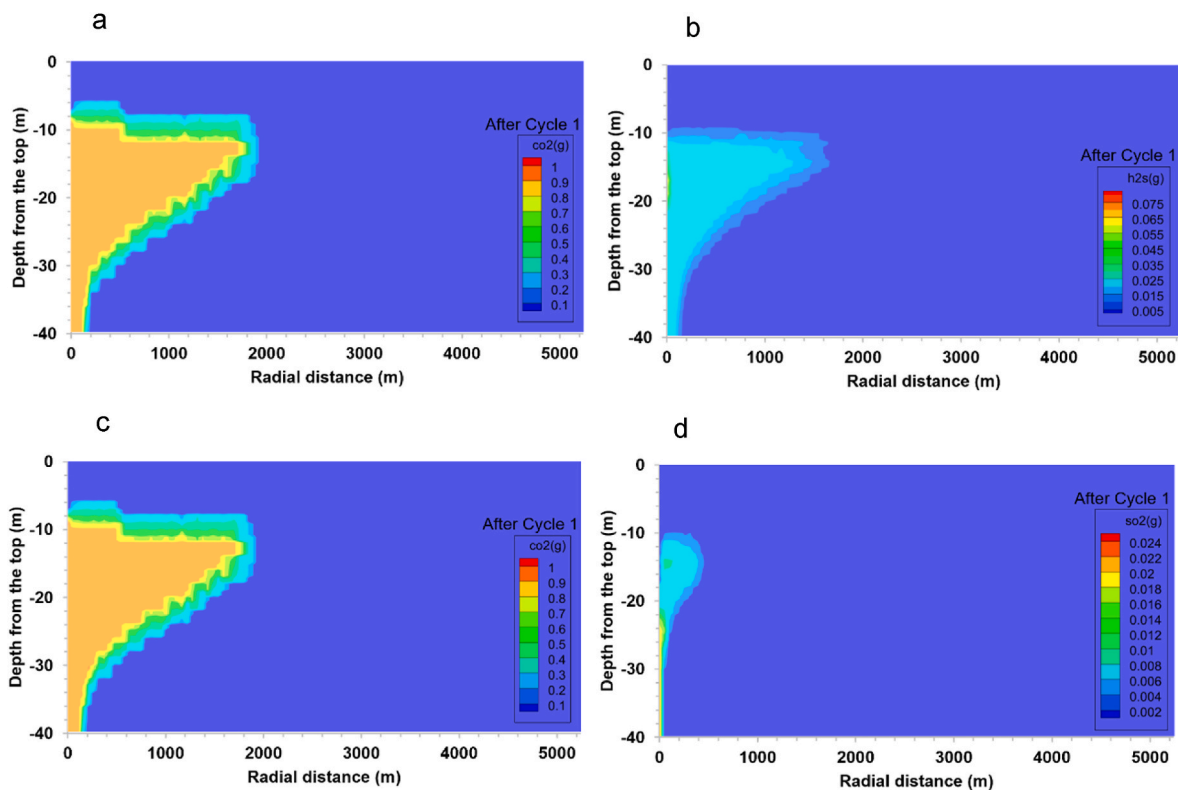


Fig. 3. Gas front of (a) CO₂ in CO₂-H₂S (b) H₂S (c) CO₂ in CO₂-SO₂ (d) SO₂ in cyclic process.

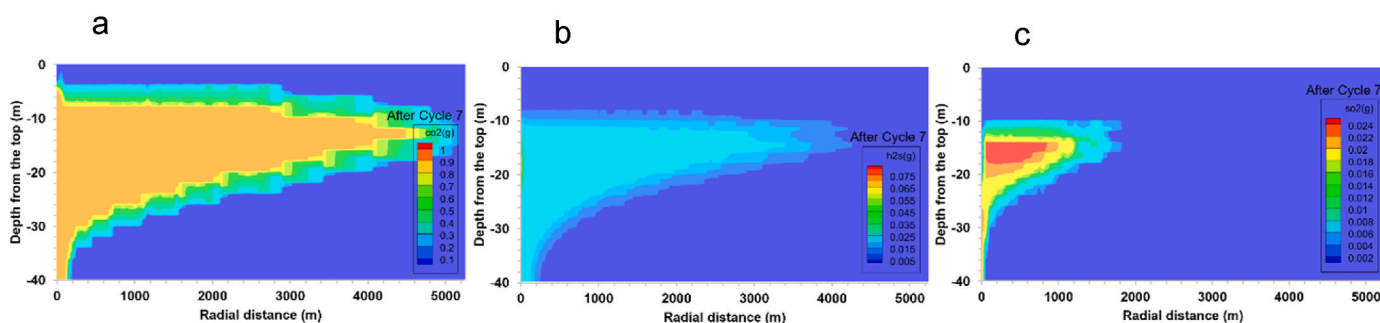


Fig. 4. (a) CO₂ gas (b) H₂S gas (c) SO₂ gas in the formation after seven cyclic injection-withdrawal process.

carbon (TDC) for the geosequestration cases (after seven cyclic injection-withdrawal process of fluid), as the initially displaced formation water during supercritical fluid injection flows towards the injection-production well and provides sufficient pressure needed for the gas production. Thus, convective mixing of the CO₂ with formation water during the withdrawal process might have made the TDC for all

the injection cases similar. It is also possible that some residually trapped CO₂ might have reconnected with the injected CO₂ in subsequent injection cycles mainly close to the large pore clusters, as [Lysy et al. \(2023\)](#) observed for hydrogen during cyclic hydrogen (H₂) injections. The concentration of dissolved CO₂ increased up to 0.9 mol/kg H₂O in the two-phase region due to the CO₂ gas migration ([Fig. 5](#)). The

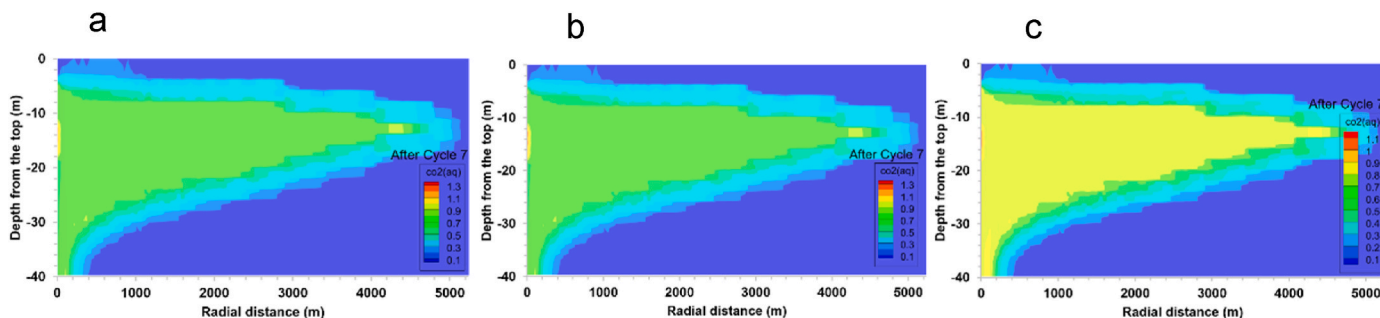


Fig. 5. TDC for (a) CO₂ alone (b) CO₂-H₂S (c) CO₂-SO₂ cases in the formation after seven (7) cyclic injection-withdrawal process.

dissolution of the injected CO₂ (with or without cases of H₂S or SO₂ gas co-injection) in the surrounding formation water yields H₂CO₃, HCO₃⁻, and CO₃²⁻, and decreases pH (increases acidity). The pH profiles of all the injection cases are similar, as shown in Fig. 6. However, for the CO₂-SO₂ co-injection case, the pH of the reservoir at and near the perforations in the production zone is relatively very low compared to the other injection cases. This could be attributed to severe calcite dissolution in those regions resulting in very low pH. In other regions of the formations, the pH values are similar for all the injection cases.

The low pH induces the dissolution and precipitation of minerals. Dissolution of the minerals increases concentrations of cations including Na⁺, Ca²⁺, Mg²⁺, and Fe²⁺, which then form aqueous complexes with the carbonate ions and further precipitation of minerals (including secondary minerals). Examples of such aqueous complexes are NaHCO₃, CaHCO₃⁺, MgHCO₃⁺, and FeHCO₃⁺; and examples of precipitated secondary minerals are ankerite, dawsonite, siderite, smectite-Na, pyrite, and anhydrite (CO₂-SO₂ co-injection case). As the aqueous complexes are formed, more CO₂ goes into the solution and enhances solubility trapping. However, mineral trapping of CO₂ was not considered in this study as it is a slow process that occurs over hundreds to thousands of years, while the numerical simulations in this study were performed up to a maximum of 87.5 years. So, the CO₂ trapping mechanisms in the present study are structural/stratigraphic trapping (caprock), residual trapping, and solubility trapping.

Minerals such as anhydrite, albite, chlorite, illite, k-feldspar, and kaolinite in the shale formation dissolve in the two-phase region and near the front of the single aqueous-phase zone. The mineral reactions are consistent with the findings in the study conducted (up to 5000 years of sequestration) by Ma et al. (2019). Calcite, albite, chlorite, and k-feldspar in sandstone reservoir dissolve in the two-phase region and near the front of the single aqueous-phase zone. On the other hand, calcite, ankerite, quartz, siderite, smectite-Ca, smectite-Na, and small amounts of hematite and pyrite precipitated in the shale caprock; while illite, kaolinite, quartz, and smectite-Na precipitated in the sandstone reservoir during the cyclic injection and withdrawal of CO₂ (Figs. 7–10). For the CO₂-H₂S co-injection case, pyrite precipitated in the sandstone reservoir and shale caprock; while for the CO₂-SO₂ co-injection case, anhydrite, pyrite, and a small amount of dawsonite precipitated in the shale and sandstone formations. This result is in line with the findings of Zhang et al. (2011), and the precipitation of ankerite and siderite can be attributed to the fact that Fe²⁺ is required and supplied by the dissolution of iron-bearing minerals such as chlorite. Very large amount of calcite dissolved in the CO₂-SO₂ case compared to the other injection cases. In fact, complete to significant dissolution of calcite mineral was observed at and near the perforations in the production zone for all the injection cases. Thus, erosion of the calcite mineral during CO₂ withdrawal resulted in the deposition of some of the calcite mineral in reservoir layers directly below the perforation interval in the production zone. Consequently, the porosity of those few reservoir layers directly below the perforation interval in the production zone decreased during the CO₂ geosequestration. Moreover, the large amount of calcite dissolution at and near the perforation interval of the production zone

resulted in significant precipitation of anhydrite in that region for the CO₂-SO₂ co-injection case. Changes in the composition (volume fraction of the solid rock) of calcite, anhydrite, and pyrite during the cyclic process of the CO₂ geosequestration are shown in Fig. 7.

Changes in porosity are calculated from variations in the volume fraction of the minerals, while the permeability ratios are calculated by the changes in the porosity using the Kozeny-Carman relation. In the two-phase region, due to dominant mineral dissolution caused by low pH, porosity increases slightly in the shale and sandstone rocks, in the cases of CO₂ alone and CO₂-H₂S co-injection, while in the case of CO₂-SO₂ co-injection, porosity increases in most part of the shale rock (except in the layer contacted by SO₂ and where anhydrite precipitated) and decreases in the sandstone reservoir due to anhydrite precipitation.

For the CO₂-SO₂ co-injection case, at the perforations in the production zone, the reservoir porosity increased and it is between 0.36120 and 0.36672, while in every other region where SO₂ dissolved in water, porosity decreased (the lowest porosity observed is 0.32496). Beyond the regions contacted by SO₂ (mainly dissolved CO₂), porosity increased up to 0.34891 (the corresponding permeability increase is 11.05%). In the shale caprock, porosity decreased in the layer contacted by SO₂ (about 2 m vertical thickness); in other areas of the caprock contacted mainly by CO₂, porosity increased slightly. For the CO₂-H₂S co-injection case, at the perforations in the production zone, porosity increased and it is between 0.36018 and 0.36031. From the lower perforation layer at the perforation zone down to 2–6 m vertical thickness and up to about 7 m lateral distance in the reservoir, porosity decreased. This decrease in porosity can be attributed to the deposition of fines or minerals due to the erosion of some minerals or rock materials in the production zone during CO₂ gas withdrawal from the perforation interval. This result is in line with the submission of Saedi et al., (2011) that rocks susceptible to formation damage (including fines migration) may experience reduced injectivity during cyclic CO₂-brine injection, even though the level of damage would stabilize after several cycles of injection. However, porosity increased in other areas contacted by CO₂. For the CO₂ alone case, at the perforations in the production zone, porosity increased and it is between 0.36019 and 0.36032. From the lower perforation layer at the perforation zone down to 2–6 m vertical thickness and up to about 9m lateral distance in the reservoir, porosity decreased, while porosity increased in other areas contacted by CO₂. In all the injection cases, the porosity and permeability of the shale caprock decreased slightly in the regions that were not contacted by any of the gases. The porosity and corresponding changes in the permeability of the formations are shown in Table 10 and Fig. 11.

After seven (7) cycles of CO₂ injection and withdrawal, for the CO₂ alone case, the maximum increase in porosity is 0.19% and 5.98% (corresponding to permeability increase of 0.59% and 26.70%) in the shale caprock and sandstone reservoir, respectively; while the maximum decrease in porosity is 0.03% and 1.56% (corresponding to permeability decrease of 0.10% and 6.12%) in the caprock and reservoir, respectively (Table 11). Similarly, for the CO₂-H₂S co-injection case, the maximum increase in porosity is 0.21% and 5.97% (corresponding to permeability increase of 0.66% and 26.68%) in the shale caprock and sandstone

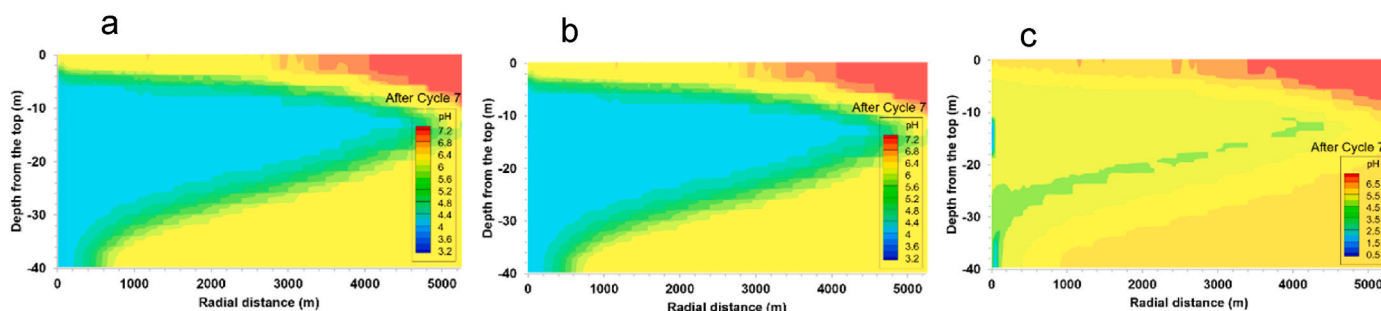


Fig. 6. pH for (a) CO₂ alone (b) CO₂-H₂S (c) CO₂-SO₂ cases in the formation after seven (7) cyclic injection-withdrawal process.

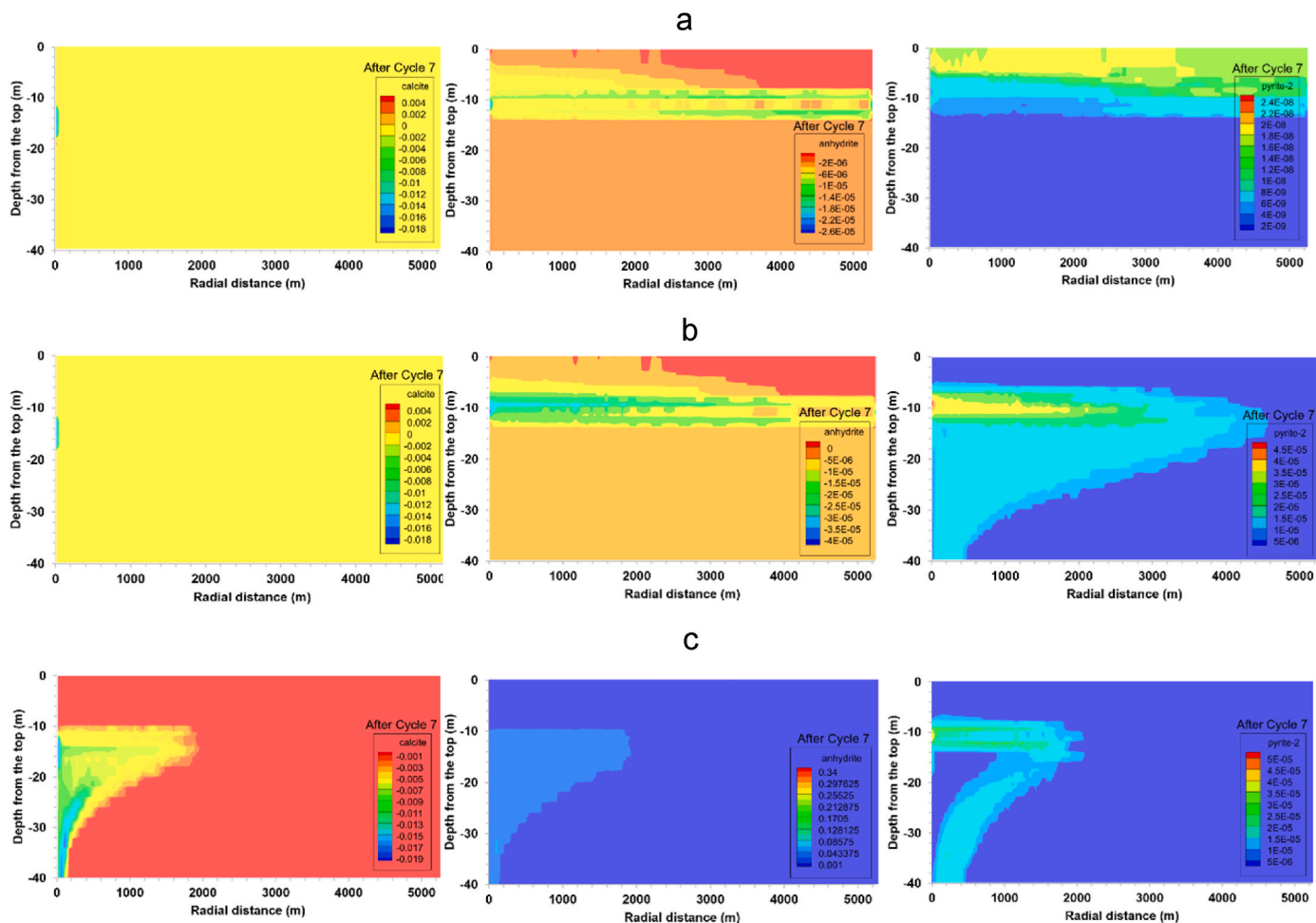


Fig. 7. Changes in calcite, anhydrite, and pyrite composition for (a) CO_2 alone (b) $\text{CO}_2\text{-H}_2\text{S}$ (c) $\text{CO}_2\text{-SO}_2$ injection cases in the formations after seven (7) cyclic injection-withdrawal process.

reservoir, respectively; while the maximum decrease in porosity is 0.03% and 1.54% (corresponding to permeability decrease of 0.10% and 6.06%) in the caprock and reservoir, respectively. In the case of $\text{CO}_2\text{-SO}_2$ co-injection, the maximum increase in porosity is 0.13% and 7.86% (corresponding to permeability increase of 0.40% and 36.29%) in the shale caprock and sandstone reservoir, respectively; while the maximum decrease in porosity is 0.3% and 4.42% (corresponding to permeability decrease of 0.92% and 16.54%) in the caprock and reservoir, respectively. For the $\text{CO}_2\text{-SO}_2$ co-injection case, the significant increase in porosity and permeability at the perforations in the production zone can be attributed to the severe dissolution of calcite, albite, chlorite, k-feldspar, and kaolinite minerals in that region, while the significant decrease in porosity and permeability in other regions of the sandstone reservoir contacted by SO_2 can be attributed mainly to the precipitation of anhydrite. These results are consistent with the results of some scholars (Bolourinejad and Herber, 2014; Pearce et al., 2016; Aminu et al., 2018), although they investigated the non-cyclic technique of CO_2 geosequestration. However, in the studies conducted by Bolourinejad and Herber (2014) and Aminu et al. (2018), porosity and permeability decreased in the reservoir during $\text{CO}_2\text{-H}_2\text{S}$ co-injection. This result is different in the present study, as only a small amount of pyrite precipitated due to the low concentration of Fe^{2+} in the formation.

4.2. Impact of impurities on the brittleness index of the sandstone reservoir and shale caprock during CO_2 geosequestration

The brittleness of sandstone and shale formations was evaluated at temperature and pressure conditions of 40 °C and 100 bar, respectively. The brittleness index of the rocks, considering the relative level of brittleness of brittle minerals as well as the simple sum of the fraction of brittle minerals is presented in Table 12 and Table 13. Table 12 shows the brittleness index of the rocks where the same molar volume of minerals are assumed to simplify the mineralogical brittleness index equations (equivalent to brittleness index without incorporating molar volume of minerals), while Table 13 shows the brittleness index of the rocks where the molar volumes of each mineral that makes up the rock are substituted in the mineralogical brittleness index equations (equivalent to brittleness index incorporating molar volume of minerals). So, tables 12 and 13 show that the initial brittleness index of the sandstone reservoir is significantly higher than that of the shale caprock. The relatively higher brittleness of sandstone formation before CO_2 sequestration is due to the high amount of the initial quartz and feldspar minerals, and some amount of calcite.

During CO_2 geosequestration, supercritical CO_2 (with or without impurities) was injected and withdrawn in cycles (up to seven cycles) for 87.5 years. SO_2 (or H_2S) gas hardly contacted the shale caprock up to 2–4 m vertical thickness from the reservoir (very low mole fraction, as higher concentration of SO_2 or H_2S is in the reservoir due to preferential dissolution of SO_2 (or H_2S) gas in the formation water. Thus, the brittleness of the shale caprock is largely dependent on the reaction of CO_2

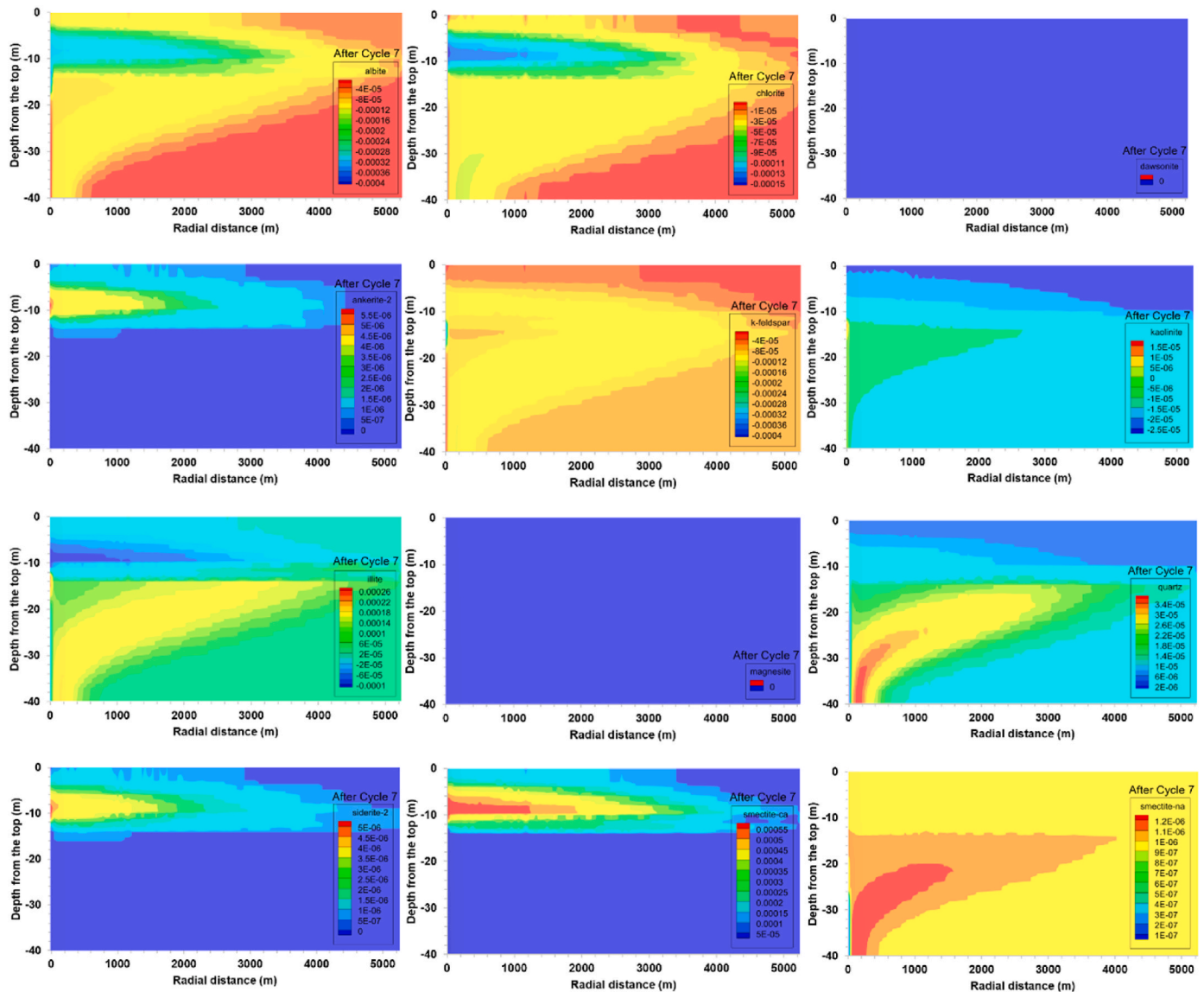


Fig. 8. Mineral dissolution and precipitation in the sandstone reservoir and shale caprock for the CO₂ alone case after seven (7) cycles of injection and withdrawal.

with the rock minerals. Hence, the brittleness of the shale caprock for all the injection cases decreased slightly during the period of CO₂ geosequestration.

Applying the brittleness index equations developed in the present study (and assuming all the minerals have the same molar volume and eliminating the molar volume parameter), the initial brittleness index (considering the relative level of brittleness of brittle minerals, BI_{bm}) of the shale caprock is 0.0377 (corresponding to brittleness index of 0.0674 using the simple sum of the fraction of brittle minerals, BI_{min}), while the initial brittleness index (BI_{bm}) of the sandstone reservoir is 0.4593 (BI_{min} = 0.8642).

In this study, the brittleness index of the rocks was evaluated mainly by considering the relative level of brittleness of brittle minerals, using BI_{bm}. For the CO₂ alone and CO₂-H₂S co-injection cases, after the first cycle of gas injection and withdrawal, the brittleness index of the shale caprock remained 0.0377 (BI_{min} = 0.0673–0.0674). At the perforations in the production zone, the brittleness index (BI_{bm}) decreased from 0.4593 to 0.4585, representing a slight change in the brittleness index. A slight increase in brittleness index from 0.4593 to 0.4594 was observed at the vertical distance up to about 0–2 m reservoir thickness below the lower production perforation layer and less than 2 m lateral distance.

The slight increase in the brittleness index might be attributed to the high amount of calcite dissolution close to the production perforations due to severe erosion of the calcite mineral as CO₂ is produced in the production zone. Hence, some fraction of the calcite (brittle mineral) is deposited at the layers slightly below the production zone. In the CO₂-SO₂ co-injection case, after the first cycle of gas injection and withdrawal, the brittleness index of the shale caprock decreased slightly to about 0.0376 at the caprock layer contacted by SO₂. At the top two production perforations the brittleness index of the reservoir is 0.4586 and at the lowest production perforation the brittleness index is 0.3457, corresponding to significantly low porosity as all calcite minerals dissolved and precipitated large amount of anhydrite in that region as that region of the perforation interval has dissolved SO₂; while notable decrease in brittleness index down to 0.4499 was observed in other areas of the reservoir contacted by SO₂. However, at the perforations and regions in the reservoir [vertically and horizontally] close to the well perforations, the brittleness index might not be accurate for all the cycles of fluid injection and withdrawal, as the dissolved minerals in those regions or minerals that are deposited below the perforation interval close to the well are mainly unconsolidated materials (wellbore instability and fines deposition). Therefore, brittleness index evaluation

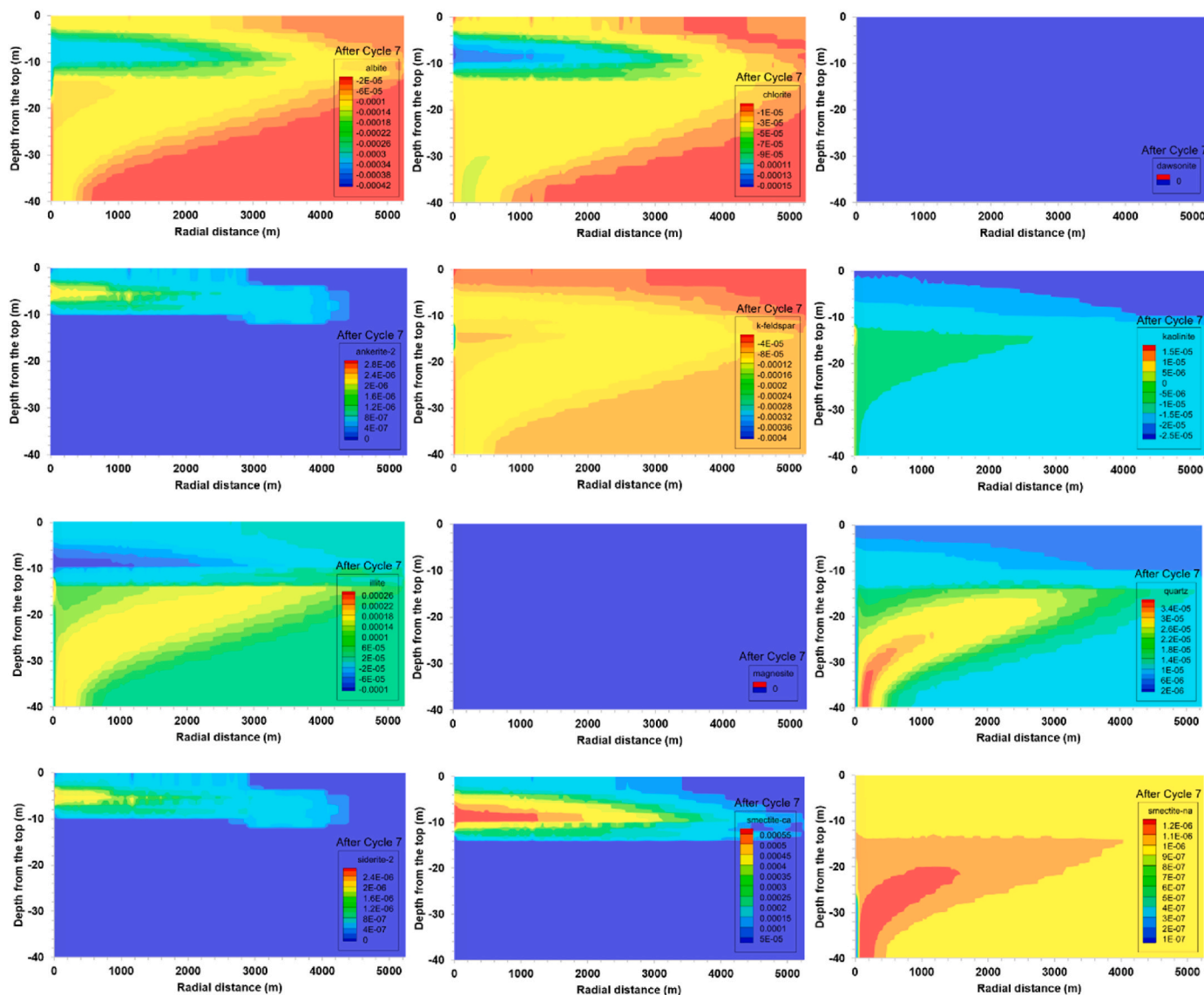


Fig. 9. Mineral dissolution and precipitation in the sandstone reservoir and shale caprock for the CO₂-H₂S case after seven (7) cycles of injection and withdrawal.

based on the mineralogical composition from the numerical simulation would be more accurate farther away from the perforations (vertically and horizontally).

In the CO₂ alone and CO₂-H₂S co-injection cases, after the seventh cycle of gas injection and withdrawal, the brittleness index of the shale caprock decreased to about 0.0375. At the perforations in the production zone, the brittleness index is between 0.4582 and 0.4584, representing a negligible change in brittleness index after 75 years of CO₂ geosequestration (from the end of the first gas injection-withdrawal cycle). A slight increase in brittleness index up to 0.4594 (the same after the first cycle) was observed at the vertical distance up to about 0–4 m reservoir thickness and less than 2 m lateral distance below the lower production perforation layer. In the CO₂-SO₂ co-injection case, after the seventh cycle of gas injection and withdrawal, the brittleness index of the shale caprock decreased to about 0.0373 at the caprock layer contacted by SO₂. At the production perforations, the brittleness index of the reservoir is 0.4588 (slightly higher than the first cycle), representing a negligible change in the brittleness index. However, a significant decrease in the brittleness index to about 0.4433 was observed in other areas of the reservoir contacted by SO₂.

Table 13 shows that incorporating the different molar volumes corresponding to each mineral in the rock (which converts the volume

fraction of the minerals to the actual weight fraction of the minerals and is expected to be more accurate for estimating the brittleness index of rocks if the actual molar volumes of the minerals are incorporated) gives a higher brittleness index compared to when the molar volume parameter is eliminated from the brittleness index equation.

Applying the brittleness index equations developed in the present study (and incorporating the different molar volume corresponding to each mineral in the rock), the initial brittleness index (considering the relative level of brittleness of brittle minerals, BI_{bm}) of the shale caprock is 0.1073 (corresponding to brittleness index of 0.1653 using the simple sum of the fraction of brittle minerals, BI_{min}), while the initial brittleness index (BI_{bm}) of the sandstone reservoir is 0.5892 (BI_{min} = 0.9307). The change in brittleness index in the shale caprock is similar to what is observed when the molar volume parameter is eliminated from the equation. After seven cycles of CO₂ injection and withdrawal, the brittleness index decreased to about 0.1071 (BI_{min} = 0.1649) for the CO₂ alone and CO₂-H₂S cases and decreased to about 0.1063 (BI_{min} = 0.1633) for the CO₂-SO₂ case. The percentage decrease in brittleness index (BI_{bm}) in the sandstone reservoir and shale caprock after seven cycles of injection and withdrawal for the CO₂-SO₂ case is 5.38% and 0.93%, respectively. The change in the brittleness index of the shale caprock, as well as the change in its porosity and permeability, during

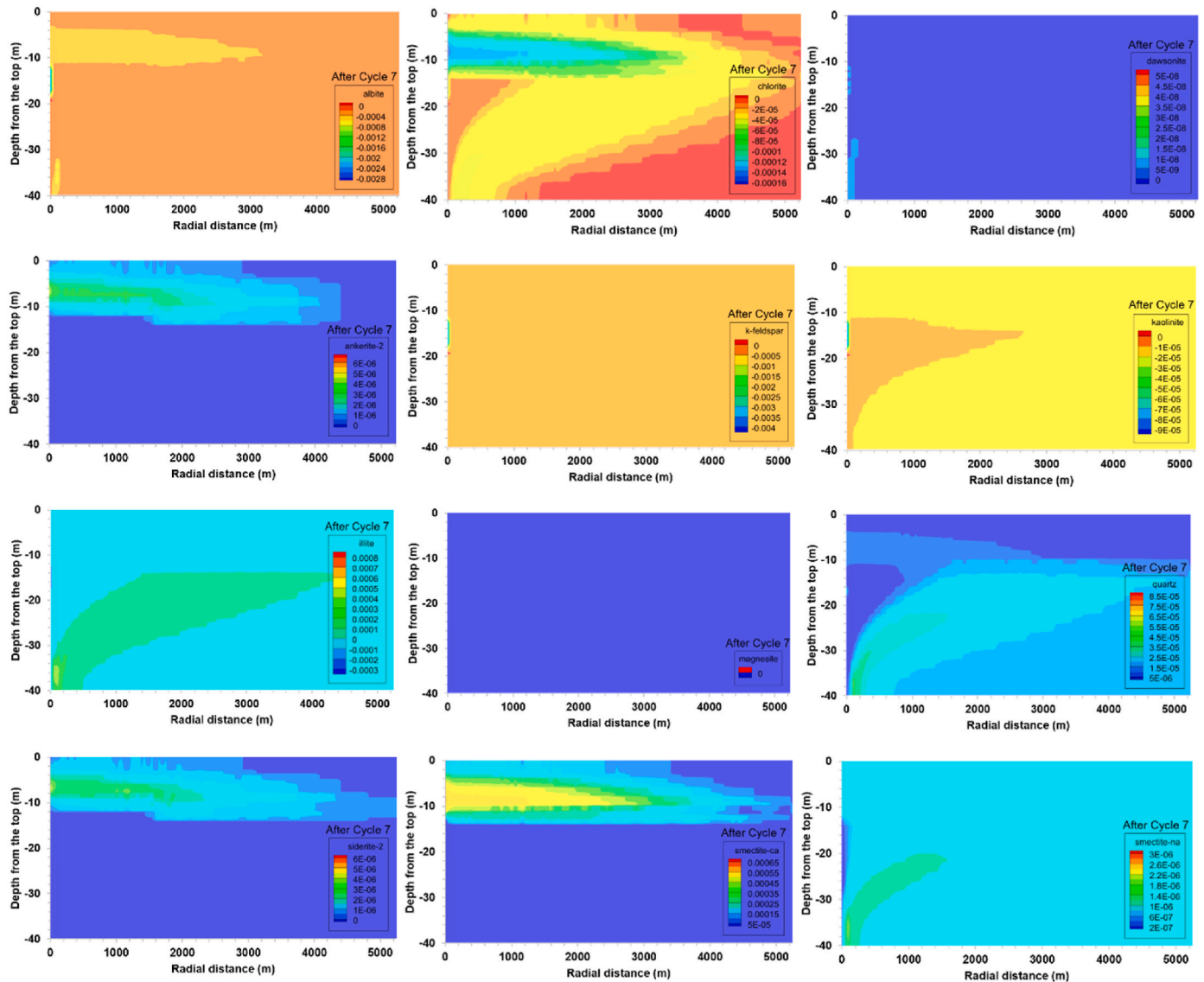


Fig. 10. Mineral dissolution and precipitation in the sandstone reservoir and shale caprock for the CO₂-SO₂ case after seven (7) cycles of injection and withdrawal.

Table 10

Porosity and permeability ratio of the formations after seven (7) cycles of CO₂ injection and withdrawal.

Formation type	Petrophysics	After Cycle 7		
		CO ₂	CO ₂ -H ₂ S	CO ₂ -SO ₂
Shale caprock	Porosity	0.06998-	0.06998-	0.06979-
	Permeability ratio	0.07013	0.07015	0.07009
Sandstone reservoir	Porosity	0.99904-	0.99903-	0.99078-
	Permeability ratio	1.00590	1.00660	1.00400
Sandstone reservoir	Porosity	0.33470-	0.33475-	0.32496-
	Permeability ratio	0.36032	0.36031	0.36672
Sandstone reservoir	Porosity	0.93881-	0.93943-	0.83462-
	Permeability ratio	1.26700	1.26680	1.36290

CO₂ geosequestration is negligible for all the cases considered. Therefore, the integrity of the caprock is maintained during cyclic CO₂ geosequestration. Overall, the decrease in brittleness of the shale caprock is consistent with the results of Lyu et al. (2018), although they adopted a non-cyclic technique of CO₂ sequestration. Lyu et al. (2018) applied the energy-balance method together with the Weibull distribution-based constitutive model to calculate the brittleness values of shale rock

samples with or without [CO₂-brine] soaking conditions. They found that CO₂-brine-shale rock interactions decrease the brittleness values of the shale rock as well as its peak axial strength and Young's modulus.

Furthermore, the change in brittleness index in the sandstone reservoir is similar to what is observed when the molar volume parameter is eliminated from the equation, except at the perforations and regions in the reservoir [vertically and horizontally] close to the well perforations where the brittleness index by the simple sum of the fraction of brittle minerals did not correspond to the brittleness index by the relative level of brittleness of brittle minerals. For all the geosequestration cases (with or without impurities), BI_{min} decreased at the perforations, while BI_{bm} increased at the perforations. For the CO₂ alone and CO₂-H₂S cases, in the regions where it appears that minerals are deposited or precipitated minerals are unconsolidated (a few layers below the perforation interval and close to the well), BI_{min} increased, while BI_{bm} decreased, except for the CO₂-SO₂ case where both BI_{min} and BI_{bm} decreased mainly due to anhydrite precipitation. So, mineralogical brittleness index models might not be accurate at the perforations and regions in the reservoir [vertically and horizontally] close to the well perforations. Therefore, XRD analysis and mechanical tests on the change in the mineralogical and geomechanical properties of sandstone rock samples and their fracture behaviour upon treatment with pure CO₂

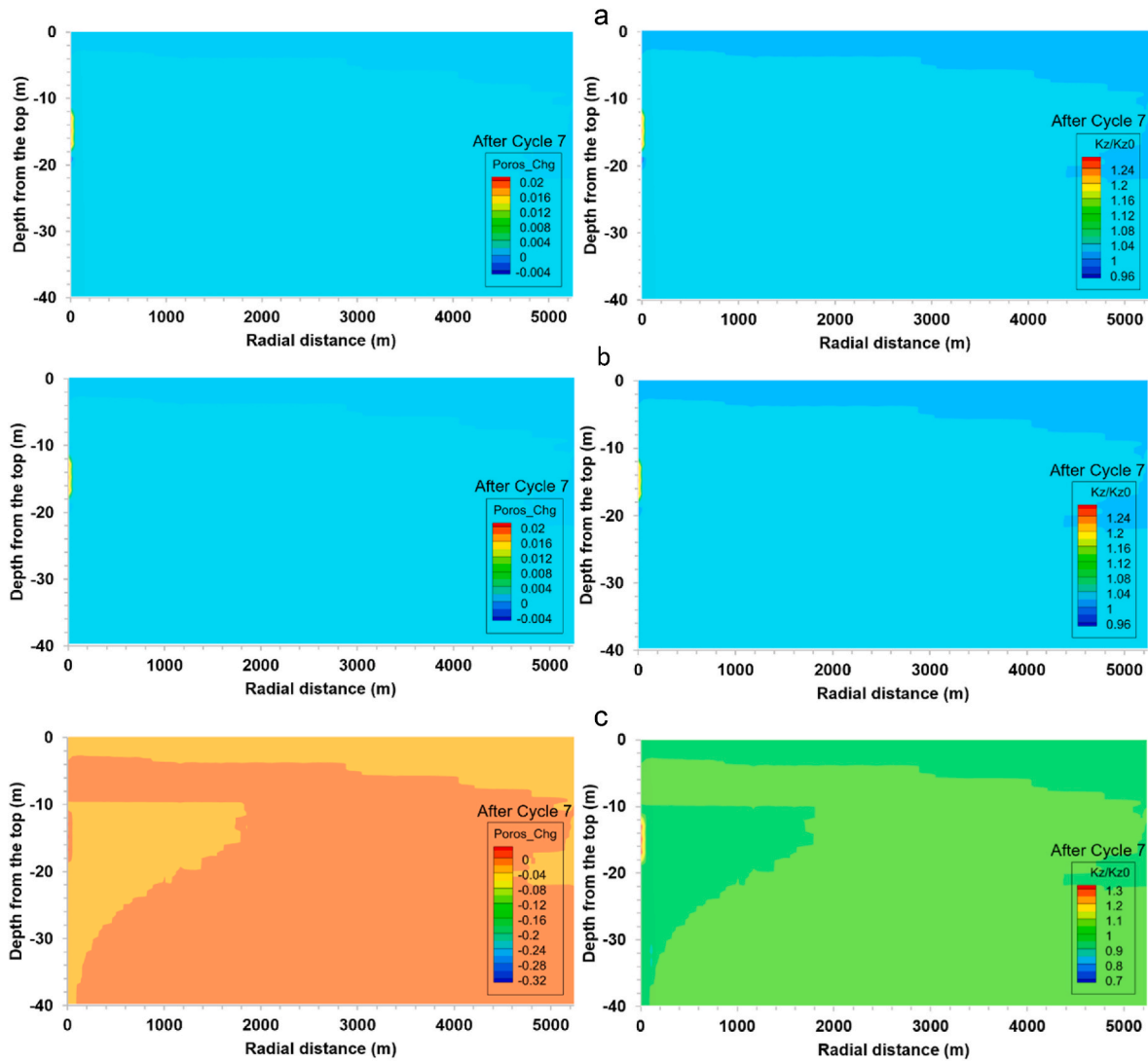


Fig. 11. Porosity changes and permeability ratios for (a) CO₂ alone (b) CO₂-H₂S (c) CO₂-SO₂ injection cases in the formations after seven (7) cyclic injection-withdrawal processes.

Table 11
Changes in porosity and permeability of the formations after seven (7) cycles of CO₂ injection and withdrawal.

Formation type	Petrophysics	After Cycle 7		
		CO ₂	CO ₂ -H ₂ S	CO ₂ -SO ₂
Shale caprock	Percentage change in porosity	-0.03-0.19	-0.03-0.21	-0.30-0.13
	Percentage change in permeability	-0.10-0.59	-0.10-0.66	-0.92-0.40
Sandstone reservoir	Percentage change in porosity	-1.56-5.98	-1.54-5.97	-4.42-7.86
	Percentage change in permeability	-6.12-26.70	-6.06-26.68	-16.54-36.29

or CO₂ mixture would be required to evaluate the correlation between the mineralogical brittleness index and mechanical brittleness index of the rock samples.

To quantify the reliable change between the brittleness index of rocks for the CO₂ alone and CO₂-SO₂ co-injection cases, the reliable

change index was computed using brittleness index results (assuming all the minerals have the same molar volume and eliminating the molar volume parameter) from the CO₂ alone and CO₂-SO₂ co-injection cases at 87.5 years. The first column contains the brittleness index for the CO₂ alone case, while the second column contains the brittleness index of rocks for the CO₂-SO₂ co-injection case (a total of 1120 rows or observations). The Pearson's correlation coefficient (reliability coefficient, *r*) is 0.999747 (representing excellent reliability of the brittleness index), and the calculated standard deviation (σ) of the distribution of the brittleness index for the CO₂ alone case is 0.220965. Therefore, the reliable change index (with 95% confidence) is 0.009745. Hence, the absolute change in brittleness index between the CO₂ alone case and the CO₂-SO₂ co-injection case greater than 0.009745 is considered significant. Therefore, in the present study, the change in the brittleness index of the sandstone reservoir for the CO₂-SO₂ co-injection case is significant.

The brittleness index calculated in this study based on the results from the numerical simulation for the CO₂ alone and CO₂-SO₂ co-injection cases were validated using an existing brittleness index model (BI_{BMod}) that utilizes the weight fraction of brittle minerals and considers relative bulk modulus of brittle minerals (Kang et al., 2020), and brittleness index model (BI₄) that considers the simple sum of weight fraction of brittle minerals, using the experimental data

Table 12Brittleness index of the formations before and after the first and seventh cycles of CO₂ injection and withdrawal (eliminating molar volume).

Formation type	Brittleness index	Before sequestration, t = 0			After cycle 1			After cycle 7		
		CO ₂	CO ₂ -H ₂ S	CO ₂ -SO ₂	CO ₂	CO ₂ -H ₂ S	CO ₂ -SO ₂	CO ₂	CO ₂ -H ₂ S	CO ₂ -SO ₂
Shale caprock	Bl _{bm}	0.0377	0.0377	0.0377	0.0377	0.0377	0.0376-	0.0375-	0.0375-	0.0373-
	Bl _{min}	0.0674	0.0674	0.0674	0.0673-	0.0673-	0.0673-	0.0671-	0.0671-	0.0666-
Sandstone Reservoir	Bl _{bm}	0.4593	0.4593	0.4593	0.4585-	0.4585-	0.3457-	0.4582-	0.4582-	0.4433-
	Bl _{min}	0.8642	0.8642	0.8642	0.8622-	0.8622-	0.6499-	0.8616-	0.8615-	0.8334-
					0.8644	0.8644	0.8642	0.8645	0.8645	0.8642

Table 13Brittleness index of the formations before and after the first and seventh cycles of CO₂ injection and withdrawal (with molar volume).

Formation type	Brittleness index	Before sequestration, t = 0			After cycle 1			After cycle 7		
		CO ₂	CO ₂ -H ₂ S	CO ₂ -SO ₂	CO ₂	CO ₂ -H ₂ S	CO ₂ -SO ₂	CO ₂	CO ₂ -H ₂ S	CO ₂ -SO ₂
Shale caprock	Bl _{bm}	0.1073	0.1073	0.1073	0.1072-	0.1072-	0.1071-	0.1071-	0.1071-	0.1063-
	Bl _{min}	0.1653	0.1653	0.1653	0.1651-	0.1651-	0.1649-	0.1649-	0.1649-	0.1633-
Sandstone Reservoir	Bl _{bm}	0.5892	0.5892	0.5892	0.5887-	0.5887-	0.3672-	0.5885-	0.5885-	0.5575-
	Bl _{min}	0.9307	0.9307	0.9307	0.5917	0.5917	0.5919	0.9312-	0.9312-	0.8749-
					0.9310-	0.9311-	0.5760-	0.9280	0.9280	0.9307
					0.9285	0.9285	0.9307	0.9280	0.9280	0.9307

published by Mavhengere et al. (2022). The estimated brittleness index using the existing models is shown in Table 14. The existing models applied to the experimental data and the model adopted in the present study (based on the molecular weight, molar volume, and volume fraction of minerals) account for the significant change in the brittleness of the sandstone reservoir when SO₂ is co-injected with CO₂. With pure CO₂, the change in the brittleness index of both ZC and ZG is negligible but changes significantly with the CO₂-SO₂ mixture.

The alteration in the mineral phases of the ZC rock sample is similar to the sandstone reservoir in the present study, as the CO₂-SO₂ mixture resulted in a decrease in brittleness index of the rock; therefore, ZC sandstone was used to validate the mathematical model in the present study. Unlike ZC, for ZG, smectite (clay mineral) and stilbite dissolution were observed, while plagioclase and calcite precipitated, thereby inhibiting the precipitation of gypsum and increasing the brittleness index in the CO₂-SO₂ mixture case. The difference in the chemical reaction in the ZC and ZG sandstones is due to their mineralogical composition. For example, the ZG rock sample does not have calcite, pyrite, and diopside as primary minerals; whereas those are some of the primary minerals in ZC rock sample. Hence, only gypsum precipitated as a secondary mineral in ZC rock sample, while calcite precipitated as a secondary mineral in the ZG rock sample. Therefore, the impact of contaminants on the brittleness index of rocks depends on their (rocks') mineralogical composition. Furthermore, although the samples (sandstone samples from Zululand Basin) were held in the reactors in the CO₂ and gas mixture only for 2 months, this analysis confirms that the change in the brittleness index of rocks during the storage of pure CO₂ is negligible compared to how much CO₂-SO₂ mixture alters the brittleness of rocks.

Table 14

Brittleness index of ZC and ZG rock samples.

Sample	Bl ₄	Bl _{BMod}
ZC untreated	0.93	0.68
ZC CO ₂ treated	0.92	0.69
ZC CO ₂ -SO ₂ treated	0.79	0.63
ZG untreated	0.76	0.52
ZG CO ₂ treated	0.79	0.52
ZG CO ₂ -SO ₂ treated	0.88	0.60

However, sufficient laboratory experiments would be required to treat sandstone rock samples with CO₂-brine or CO₂-brine with gas impurities, followed by detailed XRD analyses and mechanical tests of the samples, to ascertain the change in their mineralogical and geo-mechanical properties as well as the change in their fracture behaviour. These experiments and tests could also be extended to different shale and carbonate rocks.

5. Conclusions and recommendations

5.1. Conclusions

In this study, a 2-D reactive transport model was developed for a cyclic approach of CO₂ geosequestration in a sandstone reservoir overlain by shale caprock. Furthermore, mathematical models were applied to evaluate the mineralogical brittleness index of the formations before and after CO₂ sequestration (with or without SO₂ or H₂S). Based on the key findings in this study, the conclusions are summarized as follows.

1. The preferential dissolution of SO₂ or H₂S gas into formation water (compared with CO₂ gas) leads to the delayed breakthrough of SO₂ or H₂S gas, and the separation between CO₂ and SO₂/H₂S gases at the moving front. In both co-injection cases, more SO₂/H₂S contains in the interior of the gas plume (during the CO₂ co-injection period, the mole fraction of SO₂/H₂S gas diminishes gradually from the injection well or perforation interval, laterally and upward as the CO₂ gas moves).
2. The total dissolved carbon (TDC) for all the geosequestration cases is nearly the same. This could be attributed to the convective mixing of the CO₂ (with or without H₂S/SO₂) with the formation water during the gas (supercritical fluid) withdrawal process, as additional pressure to produce the gas through the perforations in the production zone comes from the formation water. Thus, residually trapped CO₂ might have reconnected with the injected CO₂ in subsequent injection cycles, and water in rock pores containing dissolved H₂S or SO₂ might be flooded with water from different zones in the reservoir, enabling more CO₂ to be dissolved and resulting in a similar TDC for all the injection cases.

- In all the injection cases, the porosity and permeability of the reservoir at the perforations in the production zone increased due to the severe dissolution of calcite and dissolution of some of the primary minerals, creating more flow paths for the gas production. The porosity and permeability of the sandstone reservoir decreased in a few layers (and a small lateral distance in the reservoir) directly below the perforation interval in the production zone for all the injection cases. This decrease in porosity and permeability could be attributed to the deposition of dissolved (or eroded) minerals (especially calcite) or fines from the production zone in those layers. In other regions in the reservoir, the porosity and permeability increased for the CO₂ alone and CO₂-H₂S co-injection cases and decreased for the CO₂-SO₂ co-injection case.
- The brittleness index of the sandstone reservoir and shale caprock decreased for all the injection cases, except at the perforations and regions in the reservoir [vertically and horizontally] close to the well perforations where the brittleness index models cannot account for accurately as the minerals in that region might constitute unconsolidated materials. A significant change (or decrease) in the brittleness index of the formations was observed only in the CO₂-SO₂ co-injection case due to a significant amount of anhydrite precipitation. The change in brittleness index in the formations for the CO₂ alone and CO₂-H₂S co-injection cases is negligible. Also, the change in brittleness index of the shale caprock, as well as its change in porosity and permeability during the cyclic CO₂ geosequestration is negligible. Therefore, the integrity of the caprock is maintained during CO₂ geosequestration (with or without the addition of small amount of H₂S or SO₂).

5.2. Recommendations for future study

- Future studies should consider performing experiments to determine changes in the mechanical strengths (compressive and tensile strengths) and fracture behaviour of rocks subjected to cyclic injection and withdrawal, and their corresponding changes in the mechanical brittleness index of the rocks during CO₂ co-injection with H₂S or SO₂ gas.
- Future studies should perform numerical simulations of cyclic injection and withdrawal over thousands of years and determine the impact of mineral trapping of CO₂, with solubility and residual trapping mechanisms, on the brittleness of rocks.
- Further studies should be conducted to investigate fines migration from the reservoir to the well or tubing string during cyclic injection and withdrawal of CO₂.

CRedit authorship contribution statement

Efenwengbe Nicholas Aminaho: Writing – review & editing, Writing – original draft, Visualization, Validation, Software, Project administration, Methodology, Investigation, Funding acquisition, Formal analysis, Data curation, Conceptualization. **Mamdud Hossain:** Writing – review & editing, Supervision. **Nadimul Haque Faisal:** Supervision. **Reza Sanaee:** Supervision.

Declaration of competing interest

The authors declare that they have no known competing financial interests or personal relationships that could have appeared to influence the work reported in this paper.

Data availability

Data will be made available on request.

Acknowledgements

The authors would like to acknowledge the flexible funding and partnership offered by the UK Carbon Capture and Storage Research Centre (UKCCSRC). This project was jointly funded by Robert Gordon University (Aberdeen) and UKCCSRC.

References

- Abedini, A., Torabi, F., 2014. On the CO₂ storage potential of cyclic CO₂ injection process for enhanced oil recovery. *Fuel* 124, 14–27.
- AL-Ameri, W.A., Abdulraheem, A., Mahmoud, M., 2016. Long-term effects of CO₂ sequestration on rock mechanical properties. *J. Energy Resour. Technol.* 138, 1–9.
- Aminaho, E.N., Hossain, M., 2023. Caprock Integrity Evaluation for Geosequestration of CO₂ in Low-Temperature Reservoirs. Robert Gordon University, Aberdeen. <https://rgu-repository.worktribe.com/output/2072081>.
- Aminu, M.D., Nabavi, S.A., Manovic, V., 2018. CO₂-brine-rock interactions: the effect of impurities on grain size distribution and reservoir permeability. *Int. J. Greenh. Gas Control* 78, 168–176.
- Bachu, S., 2002. Sequestration of CO₂ in geological media in response to climate change: road map for site selection using the transform of the geological space into the CO₂ phase space. *Energy Convers. Manag.* 43, 87–102.
- Badrouchi, N., Pu, H., Smith, S., Yu, Y., Badrouchi, F., 2022. Experimental investigation of CO₂ injection side effects on reservoir properties in ultra tight formations. *J. Petrol. Sci. Eng.* 215, 1–9.
- Blampied, N.M., 2016. Reliable change & the reliable change index in the context of evidence-based practice: a tutorial review. In: Paper Presented at the NZPpS Conference, Wellington, 2–4 September 2016.
- Bolourinejad, P., Herber, R., 2014. Experimental and modelling study of storage of CO₂ and impurities in a depleted gas field in northeast Netherlands. *Energy Proc.* 63, 2811–2820.
- Deer, D.A., Howie, R.A., Zussman, J., 1966. An Introduction to the Rock Forming Minerals. Longman Scientific & Technical, Essex.
- Edlmann, K., Hinchliffe, S., Heinemann, N., Johnson, G., Ennis-King, J., McDermott, C.I., 2019. Cyclic CO₂-H₂O injection and residual trapping: implications for CO₂ injection efficiency and storage security. *Int. J. Greenh. Gas Control* 80, 1–9.
- Elwegaa, K., Emadi, H., Soliman, M., Gamadi, T., Elsharafi, M., 2019. Improving oil recovery from shale oil reservoirs using cyclic cold carbon dioxide injection – an experimental study. *Fuel* 254, 115586.
- Ezema, I.C., Edelugo, S.O., Menon, A.R.R., Omah, A.D., 2015. A comparative prediction of the tensile properties of sisal fiber reinforced epoxy composite using volume fraction and mass fraction models. *Journal of Metallurgical and Materials Engineering Research* 1 (2), 9–18.
- Fatah, A., Mahmud, H.B., Bennour, Z., Gholami, R., Hossain, M., 2022. Geochemical modelling of CO₂ interactions with shale: Kinetics of mineral dissolution and precipitation on geological time scales. *Chemical Geology* 592, 120742. <https://doi.org/10.1016/j.chemgeo.2022.120742>.
- Fatima, S., Khan, H.M.M., Tariq, Z., Abdalla, M., Mahmoud, M., 2021. An experimental and simulation study of CO₂ sequestration in underground formations: impact on geomechanical and petrophysical properties. In: Paper (SPE-204726-MS) Presented at the SPE Middle East Oil & Gas Show and Conference. November 28–December 1, 2021.
- Fjaer, E., Holt, R.M., Horsrud, P., Raaen, A.M., Risnes, R., 2008. Petroleum related rock mechanics. *Developments in Petroleum Science*, 53. second ed. Elsevier, Amsterdam.
- Gong, Q.M., Zhao, J., 2007. Influence of rock brittleness on TBM penetration rate in Singapore granite. *Tunn. Undergr. Space Technol.* 22 (3), 317–324.
- Guo, L., Jiang, Z., Liang, C., 2016. Mineralogy and shale gas potential of lower silurian organic-rich shale at the southeastern margin of sichuan basin, South China. *Oil Shale* 33 (1), 1–17.
- Hedayati, M., Wigston, A., Wolf, J.L., Rebscher, D., Niemi, A., 2018. Impacts of SO₂ gas impurity within a CO₂ stream on reservoir rock of a CCS pilot site: experimental and modelling approach. *Int. J. Greenh. Gas Control* 70, 32–44. <https://doi.org/10.1016/j.ijggc.2018.01.003>.
- Herring, A.L., Anderson, L., Wildenschild, D., 2016. Enhancing residual trapping of supercritical CO₂ via cyclic injections. *Geophys. Res. Lett.* 43 (18), 9677–9685.
- Hou, B., Zeng, Y., Fan, M., Li, D., 2018. Brittleness evaluation of shale based on the Brazilian splitting test. *Geofluids* 2018, 1–11.
- Hucka, V., Das, B., 1974. Brittleness determination of rocks by different methods. *Int. J. Rock Mech. Min. Sci. & Geomech* 11, 389–392.
- Jin, X., Shah, S.N., Roegiers, J.-C., Zhang, B., 2015. An integrated petrophysics and geomechanics approach for fracability evaluation in shale reservoirs. *SPE J.* 20 (3), 518–526.
- Kang, Y., Shang, C., Zhou, H., Huang, Y., Zhao, Q., Deng, Z., Wang, H., Ma, Y.Z., 2020. Mineralogical brittleness index as a function of weighting brittle minerals—from laboratory tests to case study. *J. Nat. Gas Sci. Eng.* 77, 1–9.
- Ke, Q., Li, C., Yao, W., Fan, Y., Zhan, H., Li, B., Zhang, X., 2023. Comparative characterization of sandstone microstructure affected by cyclic wetting-drying process. *Int. J. Rock Mech. Min. Sci.* 170, 1–10.
- Kim, C., Kim, J., Joo, S., Bu, Y., Liu, M., Cho, J., Kim, G., 2018. Efficient CO₂ utilization via a hybrid Na-CO₂ system based on CO₂ dissolution. *iScience* 9, 278–285.
- Klokov, A., Treviño, R.H., Meckel, T.A., 2017. Diffraction imaging for seal evaluation using ultra high resolution 3D seismic data. *Mar. Petrol. Geol.* 82, 85–96.

- Koomson, S., Park, S., Kim, W., No, C., Lee, C., Choi, H., Lee, C.-G., 2023. Electrochemical hydrogen production using captured CO₂ in alkaline solution. *Int. J. Electrochem. Sci.* 18, 1–7.
- Lasaga, A.C., Soler, J.M., Ganor, J., Burch, T.E., Nagy, K.L., 1994. Chemical weathering rate laws and global geochemical cycles. *Geochem. Cosmochim. Acta* 58, 2361–2386.
- Li, C., Zhang, F., Lyu, C., Hao, J., Song, J., Zhang, S., 2016. Effects of H₂S injection on the CO₂-brine-sandstone interaction under 21 MPa and 70 °C. *Mar. Pollut. Bull.* 106, 17–24.
- Li, D., Saraji, S., Jiao, Z., Zhang, Y., 2021. CO₂ injection strategies for enhanced oil recovery and geological sequestration in a tight reservoir: an experimental study. *Fuel* 284, 1–11.
- Li, G., Jin, Z., Li, X., Liu, K., Yang, W., Qiao, M., Zhou, T., Sun, X., 2023. Experimental study on mechanical properties and fracture characteristics of shale layered samples with different mineral components under cyclic loading. *Mar. Petrol. Geol.* 150, 1–14.
- Li, H., 2022. Research progress on evaluation methods and factors influencing shale brittleness: a review. *Energy Rep.* 8, 4344–4358.
- Liu, Y., Ma, T., Wu, H., Chen, P., 2020. Investigation on mechanical behaviors of shale cap rock for geological energy storage by linking macroscopic to mesoscopic failures. *J. Energy Storage* 29, 1–15.
- López-Rendón, R., Alejandre, J., 2008. Molecular dynamics simulations of the solubility of H₂S and CO₂ in water. *J. Mex. Chem. Soc.* 52 (1), 88–92.
- Luan, X., Di, B., Wei, J., Li, X., Qian, K., Xie, J., Ding, P., 2014. Laboratory Measurements of Brittleness Anisotropy in Synthetic Shale with Different Cementation. In: Presented at the SEG Denver 2014 Annual Meeting.
- Lysyy, M., Liu, N., Solstad, C.M., Fernø, M.A., Erslund, G., 2023. Microfluidic hydrogen storage capacity and residual trapping during cyclic injections: implications for underground storage. *Int. J. Hydrogen Energy*. <https://doi.org/10.1016/j.ijhydene.2023.04.253>.
- Lyu, Q., Long, X., Ranjith, P.G., Tan, J., Kang, Y., Luo, W., 2018. A damage constitutive model for the effects of CO₂-brine-rock interactions on the brittleness of a low-clay shale. *Geofluids* 1–14.
- Ma, X., Yang, G., Li, X., Yu, Y., Dong, J., 2019. Geochemical modelling of changes in caprock permeability caused by CO₂-brine-rock interactions under the diffusion mechanism. *Oil & Gas Science and Technology - Rev. IFP Energies Nouvelles* 74 (83), 1–13.
- “The product solid phases” in geological sequestration of carbon dioxide: thermodynamics, kinetics, and reaction path modelling. In: Marini, L. (Ed.), 2007. *Developments in Geochemistry*, vol. 11, pp. 79–167. [https://doi.org/10.1016/S0921-3198\(06\)80025-6](https://doi.org/10.1016/S0921-3198(06)80025-6).
- Mavhengere, P., Wagner, N., Malumbazo, N., 2022. Influences of SO₂ contamination in long term supercritical CO₂ treatment on the physical and structural characteristics of the Zululand Basin caprock and reservoir core samples. *J. Petrol. Sci. Eng.* 215, 1–15.
- Meng, F., Zhou, H., Zhang, C., Xu, R., Lu, J., 2015. Evaluation methodology of brittleness of rock based on post-peak stress-strain curves. *Rock Mech. Rock Eng.* 48, 1787–1805.
- Miri, R., Aagaard, P., Hellevang, H., 2014. Examination of CO₂-SO₂ solubility in water by SAFT1: implications for CO₂ transport and storage. *J. Phys. Chem. B* 118, 10214–10223.
- Panfilov, M., 2016. Underground and pipeline hydrogen storage. In: Ram, B., et al. (Eds.), *Compendium of Hydrogen Energy*, vol. 2. Woodhead Publishing, pp. 91–115. <https://doi.org/10.1016/B978-1-78242-362-1.00004-3>.
- Pearce, J.K., Dawson, G.K.W., Law, A.C.K., Biddle, D., Golding, S.D., 2016. Reactivity of micas and cap-rock in wet supercritical CO₂ with SO₂ and O₂ at CO₂ storage conditions. *Appl. Geochem.* 72, 59–76.
- Pearce, J.K., Kirste, D.M., Dawson, G.K.W., Rudolph, V., Golding, S.D., 2019. Geochemical modelling of experimental O₂-SO₂-CO₂ reactions of reservoir, cap-rock, and overlying cores. *Appl. Geochem.* 109, 1–19.
- Pruess, K., 2004. The TOUGH Codes - a family of simulation tools for multiphase flow and transport processes in permeable media. *Vadose Zone J.* 3, 738–746.
- Reeves, S., 2001. Geologic sequestration of CO₂ in deep, unmineable coalbeds: an integrated research and commercial-scale field demonstration project. *First National Carbon Sequestration Conference*. U.S.DOE/NETL, pp. 1–12.
- Rickman, R., Mullen, M., Petre, E., Grieser, B., Kundert, D., 2008. A practical use of shale petrophysics for stimulation design optimization: All shale plays are not clones of the Barnett Shale. *Society of Petroleum Engineers*.
- Robie, R.A., Bethke, P.M., Beardsley, K.M., 1967. *Selected X-Ray Crystallographic Data Molar Volumes, and Densities of Minerals and Related Substances*. United States Government Printing Office, Washington, pp. 42–72.
- Saeedi, A., Rezaee, R., Evans, B., Clennell, B., 2011. Multiphase flow behaviour during CO₂ geo-sequestration: Emphasis on the effect of cyclic CO₂-brine flooding. *J. Petrol. Sci. Eng.* 79 (3–4), 65–85.
- Sánchez-Díaz, Á., 2017. MefCO₂ – synthesis of methanol from captured carbon dioxide using surplus electricity (EU-H2020). *Impact* 2017 (5), 6–8.
- Schifflechner, C., Wieland, C., Spliethoff, H., 2022. CO₂ plume geothermal (CPG) systems for combined heat and power production: an evaluation of various plant configurations. *J. Therm. Sci.* 31 (5), 1266–1278.
- Shafiq, M.U., Mahmud, H.K.B., Wang, L., Abid, K., Gishkori, S.N., 2022. Comparative elemental and microscopic investigation of sandstone matrix acidizing at HPHT conditions. *Petroleum Research* 7, 448–458.
- Shen, X., Kolluru, G.K., Yuan, S., Kevil, C.G., 2015. Measurement of H₂S in vivo and in vitro by the monobromobimane method. In: Cadenas, E., Packer, L. (Eds.), *Methods in Enzymology*, vol. 554. Academic Press, pp. 31–45. <https://doi.org/10.1016/bs.mie.2014.11.039>.
- SNC-Lavalin Inc, 2004. *Impact of impurities on CO₂ capture, transport and storage*. IEA Greenhouse Gas R&D Programme Report (No. PH4/32).
- Sollai, S., Porcu, A., Tola, V., Ferrara, F., Pettinau, A., 2023. Renewable methanol production from green hydrogen and captured CO₂: a techno-economic assessment. *J. CO₂ Util.* 68, 1–12.
- Su, E., Liang, Y., Chang, X., Zou, Q., Xu, M., Sasmito, A.P., 2020. Effects of cyclic saturation of supercritical CO₂ on the pore structures and mechanical properties of bituminous coal: an experimental study. *J. CO₂ Util.* 40, 1–12.
- Su, E., Liang, Y., Zou, Q., 2021. Structures and fractal characteristics of pores in long-flame coal after cyclical supercritical CO₂ treatment. *Fuel* 286, 1–12.
- Sun, Y., Li, Q., Yang, D., Liu, X., 2016. Laboratory core flooding experimental systems for CO₂ geosequestration: an updated review over the past decade. *J. Rock Mech. Geotech. Eng.* 8, 113–126.
- Totten, M.W., Hanan, M.A., Knight, D., Borges, J., 2002. Characteristics of mixed-layer smectite/illite density separates during burial diagenesis. *Am. Mineral.* 87, 1571–1579.
- Wang, D., Li, J., Meng, W., Liao, Z., Yang, S., Hong, X., Zhou, H., Yang, Y., Li, G., 2023. A near-zero carbon emission methanol production through CO₂ hydrogenation integrated with renewable hydrogen: process analysis, modification and evaluation. *J. Clean. Prod.* 412, 1–15.
- Wang, H., Zhang, L., Lei, H., Wang, Y., Liu, H., Li, X., Su, X., 2021. Potential for uranium release under geologic CO₂ storage conditions: the impact of Fe(III). *Int. J. Greenh. Gas Control* 107, 103266. <https://doi.org/10.1016/j.ijggc.2021.103266>.
- Wang, J., Zhao, Y., An, Z., Shabani, A., 2022. CO₂ storage in carbonate rocks: an experimental and geochemical modelling study. *J. Geochem. Explor.* 234, 1–14.
- Wang, L., Zhang, Y., Liu, Y., Xie, H., Xu, Y., Wei, J., 2020. SO₂ absorption in pure ionic liquids: solubility and functionalization. *J. Hazard Mater.* 392, 122504 <https://doi.org/10.1016/j.jhazmat.2020.122504>.
- Wei, X.C., Li, Q., Li, X.-Y., Sun, Y.-K., Liu, X.H., 2015. Uncertainty analysis of impact indicators for the integrity of combined caprock during CO₂ geosequestration. *Eng. Geol.* 196, 37–46.
- Xu, J., Zhai, C., Ranjith, P.G., Sun, Y., Cong, Y., Zheng, Y., Tang, W., Yang, W., 2021. Investigation of non-isothermal effect of cyclic carbon dioxide on the petrography of coals for coal mine methane recovery. *Fuel* 290, 1–12.
- Xu, T., Sonnenthal, E., Spycher, N., Pruess, K., 2006. TOUGHREACT: a simulation program for non-isothermal multiphase reactive geochemical transport in variably saturated geologic media. *Comput. Geosci.* 32, 145–165. <https://doi.org/10.1016/j.cageo.2005.06.014>.
- Xu, T., Sonnenthal, E., Spycher, N., Zheng, L., 2014. TOUGHREACT V3.0-OMP Reference Manual: A Parallel Simulation Program for Non-isothermal Multiphase Geochemical Reactive Transport.
- Zhang, D., Ranjith, P.G., Perera, M.S.A., 2016. The brittleness indices used in rock mechanics and their application in shale hydraulic fracturing: a review. *J. Petrol. Sci. Eng.* 143, 158–170.
- Zhang, W., Xu, T., Li, Y., 2011. Modeling of fate and transport of co-injection of H₂S with CO₂ in deep saline formations. *J. Geophys. Res.* 116, B02202. <https://doi.org/10.1029/2010JB007652>.
- Zheng, L., Apps, J.A., Zhang, Y., Xu, T., Birkholzer, J.T., 2009. On mobilization of lead and arsenic in groundwater in response to CO₂ leakage from deep geological storage. *Chem. Geol.* 268 (3–4), 281–297.